雑誌　（王　英正）

発表者氏名	論文タイトル名	発表誌名	巻号	ページ	出版年
Oh H, Chi X, Bradfute SB, Mishina Y, Pocius J, Michael LH, Behringer RR, Schwartz RJ, Entman ML, Schneider MD.	Cardiac muscle plasticity in adult and embryo by heart-derived progenitor cells	**Annu. NY. Acad. Sci.**	１０１５	１８２－９	２００４
Oh H, Bradfute SB, GallardoTD, Nakamura T, Gaussin V, Mishina Y, Pocius J, Michael LH, Behringer RR, Garry DJ, Entman ML, Schneider MD..	Cardiac progenitor cells from adult myocardium: homing, differentiation, and fusion after infarction	**Proc Natl Acad Sci U S A**	１００	１２３１３－８	２００３
Oh H, Wang SC, Prahash A, Sano M, Moravec CS, Taffet GE, Michael LH, Youker KA, Entman ML, Schneider MD.	Telomere attrition and Chk2 activation in human heart failure.	**Proc Natl Acad Sci U S A.**	100	378-83	2003
Sano M, Abdellatif M, Oh H, Xie M, Bagella L, Giordano A, Michael LH, DeMayo FJ, Schneider MD.	Activation and function of cyclin T-Cdk9 (positive transcription elongation factor-b) in cardiac muscle-cell hypertrophy.	**Nat Med.**	8	1310-7	2002
Oh H, Taffet GE, Youker KA, Entman ML, Overbeek PA, Michael LH, Schneider MD.	Telomerase reverse transcriptase promotes cardiac muscle cell proliferation, hypertrophy, and survival.	**Proc Natl Acad Sci U S A.**	98	10308-13	2001

雑誌　（室原　豊明）

発表者氏名	論文タイトル名	発表誌名	巻号	ページ	出版年
Shintani S, Kusano K, Ii M, Iwakura A, Heyd L, Curry C, Wecker A, Gavin M, Ma H, Kearney M, Silver M, Thorne T, Murohara T, Losordo DW.	Synergistic effect of combined intramyocardial CD34 cells and VEGF-2 gene therapy post-myocardial infarction.	***Nat. Clin. Pract. Cardiovasc. Med.***	3(Suppl 1)	1976-1987	2006
Taniguchi E, Kin M, Torimura T, Nakamura T, Kumemura M, Hanada S, Hisamoto T, Yoshida T, Kawaguchi T, Baba S, Maeyama M, Koga H, Harada M, Kumashiro R, Ueno T, Ikeda H, Imaizumi T, Murohara T, Sata M.	. Endothelial progenitor cell transplantation improves the outcome following liver injury in mice.	***Gastroenterology.***	130	521-531	2006

Kobayashi K, Kondo T, Inoue N, Aoki M, Mizuno M, Komori K, Yoshida J, Murohara T.	Combination therapy using angiopoietin-1 plasmid gene and autologous bone marrow cell implantation promotes functional angiogenesis.	***Arterioscler. Thromb. Vasc. Biol.***		In press	2006

雑誌　(尾池雄一)

発表者氏名	論文タイトル名	発表誌名	巻号	ページ	出版年
Yuasa, H., Oike, Y., Iwama, A., Nishikata, I., Sugiyama, D., Perkins, A., Mucenski, ML., Suda, T. & Morishita, K.	Oncogenic transcription factor Evi-1 regulates hematopoietic stem cell proliferation through *GATA-2* expression.	EMBO J	24	1976-1987	2005
Oike, Y., Akao, M., Yasunaga, K. Yamauchi, T., Morisada, T., Ito, Y., Urano, T., Kimura, Y., Kubota, Y., Maekawa, H., Miyamoto, T., Miyata, K., Matsumoto, S., Sakai, J., Nakagata, N., Takeya, M., Koseki, H., Kadowaki, T. & Suda, T	Angiopoietin-related growth factor (AGF) antagonizes obesity and related insulin resistance.	Nat Med	11	400-408	2005
Kubota, Y., Oike, Y., Satoh, S. Tabata, Y., Niikura, Y., Morisada, T., Akao, M., Urano, T., Ito, Y., Miyamoto, T., Nagai, N., Koh, G.Y., Watanabe, S. & Suda, T.	Cooperative interaction of Angiopoietin-like proteins 1 and 2 in zebrafish vascular development.	Proc. Natl. Acad. Sci. USA	102	13502-13507	2005

Nox1 Is Involved in Angiotensin II–Mediated Hypertension
A Study in Nox1-Deficient Mice

Kuniharu Matsuno, MS; Hiroyuki Yamada, MD, PhD; Kazumi Iwata, MS; Denan Jin, MD, PhD; Masato Katsuyama, PhD; Masato Matsuki, MD, PhD; Shinji Takai, PhD; Kiyofumi Yamanishi, MD, PhD; Mizuo Miyazaki, MD, PhD; Hiroaki Matsubara, MD, PhD; Chihiro Yabe-Nishimura, MD, PhD

Background—Increased production of reactive oxygen species (ROSs) by angiotensin II (Ang II) is involved in the initiation and progression of cardiovascular diseases. NADPH oxidase is a major source of superoxide generated in vascular tissues. Although Nox1 has been identified in vascular smooth muscle cells as a new homolog of gp91phox (Nox2), a catalytic subunit of NADPH oxidase, the pathophysiological function of Nox1-derived ROSs has not been fully elucidated. To clarify the role of Nox1 in Ang II–mediated hypertension, we generated Nox1-deficient ($^{-/Y}$) mice.

Methods and Results—No difference in the baseline blood pressure was observed between Nox1$^{+/Y}$ and Nox1$^{-/Y}$. Infusion of Ang II induced a significant increase in mean blood pressure, accompanied by augmented expression of Nox1 mRNA and superoxide production in the aorta of Nox1$^{+/Y}$, whereas the elevation in blood pressure and production of superoxide were significantly blunted in Nox1$^{-/Y}$. Conversely, the infusion of pressor as well as subpressor doses of Ang II did elicit marked hypertrophy in the thoracic aorta of Nox1$^{-/Y}$ similar to Nox1$^{+/Y}$. Administration of a nitric oxide synthase inhibitor (L-NAME) to Nox1$^{+/Y}$ did not affect the Ang II–mediated increase in blood pressure, but it abolished the suppressed pressor response to Ang II in Nox1$^{-/Y}$. Finally, endothelium-dependent relaxation and the level of cGMP in the isolated aorta were preserved in Nox1$^{-/Y}$ infused with Ang II.

Conclusions—A pivotal role for ROSs derived from Nox1/NADPH oxidase was suggested in the pressor response to Ang II by reducing the bioavailability of nitric oxide. (***Circulation.*** **2005;112:2677-2685.)**

Key Words: angiotensin ■ aorta ■ hypertension ■ hypertrophy ■ nitric oxide

Accumulating evidence indicates that angiotensin (Ang) II, the principal effector peptide of the renin-angiotensin system, plays a major role in the initiation and progression of such vascular diseases as hypertension, vascular hypertrophy, and atherosclerosis.[1] These effects of Ang II are mediated by reactive oxygen species (ROSs) generated by membrane-bound nicotinamide adenine dinucleotide phosphate (NADPH) oxidase localized in the vascular wall.[2,3] The ROSs originating from the vascular oxidase have been held responsible for endothelial dysfunction and also recognized as important signaling molecules involved in vascular remodeling.[4]

Editorial p 2585
Clinical Perspective p 2685

Early studies on the source of oxidant generation were typically limited to the prototypical NADPH oxidase of phagocytic cells, which is a multisubunit enzyme comprising a membrane-associated cytochrome b_{558} (a heterodimer of a catalytic subunit gp91phox and p22phox) and several cytosolic regulatory subunits (p47phox, p40phox, p67phox, and Rac1 or Rac2). In recent years, 4 homologs of gp91phox (Nox2), named Nox1,[5] Nox3, Nox4, and Nox5,[6] have been identified as components of nonphagocyte-type NADPH oxidase. Among these Nox isoforms expressed primarily in nonphagocyte cells, Nox1 is highly expressed in colon epithelial cells.[5] In vessels, Nox1 mRNA has been detected in vascular smooth muscle cells (VSMCs) and endothelial cells but not in adventitial cells. Conversely, the phagocyte-type subunit Nox2 is localized primarily in endothelial and adventitial cells, whereas Nox4 is abundantly expressed in all of the vessel constituents.[7–11]

Although genetic approaches have been used in recent investigations, there is a relative paucity of information on the role of Nox isoforms in Ang II–mediated vascular disor-

Received July 6, 2005; revision received August 17, 2005; accepted August 18, 2005.

From the Department of Pharmacology (K.M., K.I., M.K., C.Y.-N.), Department of Cardiovascular Medicine (H.Y., H.M.), and Department of Dermatology (M. Matsuki, K.Y.), Kyoto Prefectural University of Medicine, Kyoto; and the Department of Pharmacology, Osaka Medical College (D.J., S.T., M. Miyazaki), Osaka, Japan. Drs Matsuki and Yamanishi are now at the Department of Dermatology, Hyogo College of Medicine, Nishinomiya, Japan.

The online-only Data Supplement, which contains a table, can be found at http://circ.ahajournals.org/cgi/content/full/CIRCULATIONAHA.105.573709/DC1.

Correspondence to Chihiro Yabe-Nishimura, MD, PhD, Department of Pharmacology, Kyoto Prefectural University of Medicine, Kyoto 602-8566, Japan. E-mail nchihiro@koto.kpu-m.ac.jp

© 2005 American Heart Association, Inc.

Circulation **is available at http://www.circulationaha.org**

DOI: 10.1161/CIRCULATIONAHA.105.573709

ders.[12–14] In knockout mice genetically deficient in Nox2, the basal blood pressure was lower than wild-type counterparts, whereas Ang II–dependent hypertension was unaffected.[14,15] In the aortic media of these knockout mice, hypertrophic responses to Ang II infusion were significantly attenuated.[14] Conversely, the hypertensive response to Ang II was significantly reduced in knockout mice of p47phox, a regulatory subunit of NADPH oxidase.[16] These results suggest that Nox1 may participate in Ang II–induced hypertension, because p47phox can regulate both Nox2 and Nox1.[17] To clarify the role of the Nox1 isoform in the pathogenesis of Ang II–induced hypertension, we generated Nox1-deficient mice and administered Ang II by osmotic minipumps. We report here results indicating a pivotal role for Nox1/NADPH oxidase in the pressor response to Ang II.

Methods

Generation of Nox1-Deficient Mice

Mouse genomic clones containing the *Nox1* locus were isolated from a 129/SvJ mouse genomic library constructed in lambda FixII (Stratagene) using a murine Nox1 partial cDNA fragment as a probe. A 6.5-kb *Sac*I-*Hin*dIII fragment and a 1.0-kb *Hin*dIII-*Bam*HI fragment were cloned into pBluescript II-KS (+), a plasmid containing a neomycin (neo) expression cassette driven by the murine phosphoglycerate kinase promoter. At the 3′ end of the vector, a diphtheria toxin A fragment was included to serve as a negative selection marker. The Nox1 targeting vector was designed to replace the 1.5 kb of the genomic locus containing exon 3 to 6 with the neo cassette.

R1 embryonic stem (ES) cells were transfected with the linearized targeting vector and selected with G418. Targeted ES clones were identified by polymerase chain reaction (PCR) screening and verified by Southern hybridization using genomic probes located on the 5′ and 3′ sides of the Nox1 gene. Correctly targeted ES cells were used to make chimeric mice by aggregating the cells in E2.5 embryos and transferring the aggregated embryos to pseudopregnant females.[18] Male chimeras were crossed with C57BL/6 females to generate heterozygous mice. Heterozygous females were crossed with C57BL/6 males to obtain Nox1-deficient mice ($Nox1^{-/Y}$). The present study was performed with the approval of the Committee for Animal Research at Kyoto Prefectural University of Medicine.

Animal Model

Nox1-deficient mice and their control littermates (8 to 12 weeks old) were anesthetized with sodium pentobarbital (80 mg/kg IP). The intrascapular region was shaved, and an osmotic minipump (Alzet model 2002; Durect Corp) that contained [Val^5] angiotensin II (Sigma) or vehicle (phosphate-buffered saline, PBS) was inserted to permit subcutaneous infusion of Ang II (0.7 mg · kg^{-1} · d^{-1}). In an additional series of experiments, a subpressor dose of Ang II (0.14 mg · kg^{-1} · d^{-1}) was administered for 28 days to induce vascular hypertrophy by use of osmotic minipumps (Alzet model 2004). N^G-Nitro-L-arginine methyl ester (L-NAME) purchased from Nacalai Tesque was administered in the drinking water for 14 days (1.4 mg/d).

DHE Staining

On day 7 of Ang II administration, the thoracic aorta was dissected and snap-frozen in liquid nitrogen after being embedded in Tissue-Tek O.C.T. compound (Sakura Finetechnical Co). Unfixed frozen ring segments were cut into 30-μm-thick sections and placed on a glass slide. Dihydroethidium (DHE, 10 μmol/L, Molecular Probes) was topically applied to each tissue section and coverslipped. Slides were incubated in a light-protected humidified chamber at 37°C for 30 minutes. For the detection of ethidium bromide, a 543-nm He-Ne laser combined with a 560-nm long-pass filter was used.

Detection of Superoxide Production

Superoxide (O_2^-) production was measured with the L-012 chemiluminescence assay as described previously.[19] L-012 (Wako Pure Chemical Industries, Ltd) is a luminol derivative with high sensitivity to superoxide radicals that does not exert redox cycling itself.[20] After the infusion of Ang II for 7 days, aortic rings (0.5 cm) were dissected and incubated for 30 minutes in Krebs-HEPES buffer at 37°C. Rings were transferred to scintillation vials containing 100 μmol/L L-012 in Krebs-HEPES buffer and incubated for 5 minutes at 37°C in the dark. After incubation, chemiluminescence was measured by luminometer (Lumat LB 9507, Berthold Technologies Ltd) over a period of 10 minutes at 1-minute intervals. The L-012 chemiluminescence was expressed as relative light units per milligram of dry tissue weight per minute.

Blood Pressure and Heart Rate Measurements

Blood pressure and heart rate in conscious mice were measured by the tail-cuff system using BP98A (Softron Co). Before the osmotic pump was implanted, at least 3 days of training were conducted to accustom mice to the procedure. For each time point, 5 measurements were obtained and averaged for each mouse. Mean blood pressure (MBP) was used for all data analysis.

Real-Time PCR

The thoracic aorta of mice was dissected and snap-frozen in liquid nitrogen. Total RNA was isolated by the acid guanidinium thiocyanate/phenol/chloroform method. Real-time PCR was performed by use of the GeneAmp 5700 Sequence Detection System (Applied Biosystems) with the SuperScript III Platinum SYBR Green One-Step qRT-PCR Kit (Invitrogen Corp). The primer sequences used are shown in the Data Supplement Table (http://circ.ahajournals.org/cgi/content/full/CIRCULATIONAHA.105.573709/DC1). Dissociation curves were monitored to check the aberrant formation of primer dimers. PCR-amplified products were electrophoresed on 2% agarose gels to confirm the presence of a single band. Copy numbers were calculated on the basis of standard curves generated with genuine Nox1, Nox2, and Nox4 cDNA templates. Data were expressed as copies per microgram RNA or levels relative to day 0 (%).

Histological Analysis

After the infusion of Ang II, mice were anesthetized and perfused transcardially with 10 mL of PBS followed by 10 mL of 4% paraformaldehyde phosphate buffer under pressure (100 mm Hg). The aorta, placed in 4% formalin overnight, was processed and embedded in paraffin. Three sections (6 μm) were obtained from each descending thoracic aorta, 3 mm distal to the left subclavian artery at 500-μm intervals, and stained with elastica van Gieson stain. The medial areas and circumference of the external elastic lamina were measured by use of ImageJ software. The medial thickness was calculated by dividing the medial area by the circumference of the external elastic lamina.

Measurement of cGMP Levels

After the infusion of Ang II for 7 days, the thoracic aorta was dissected and connective tissue was removed. Vessels were immediately snap-frozen in liquid nitrogen and homogenized in ice-cold 5% trichloroacetic acid. The level of cGMP in the supernatant fraction of the homogenate was measured by an enzyme immunoassay (Cayman Chemical Co) and expressed as picomoles per milligram of the dry trichloroacetic acid precipitate.

Isolated Vascular Strip Experiments

Endothelium-dependent and -independent relaxations of the isolated vessels were measured in ex vivo organ chamber baths as described previously.[21] Briefly, after the infusion of Ang II for 7 days, mice were anesthetized, and thoracic aorta was dissected free from surrounding connective tissue. The aorta was cut into helical strips (10 mm long and 1 mm wide). The resting tension was adjusted to 0.2 g, which is optimal for induction of a maximal contraction. The strips were equilibrated for 90 minutes in organ baths containing Tyrode's solution. After equilibration, the strips were precontracted

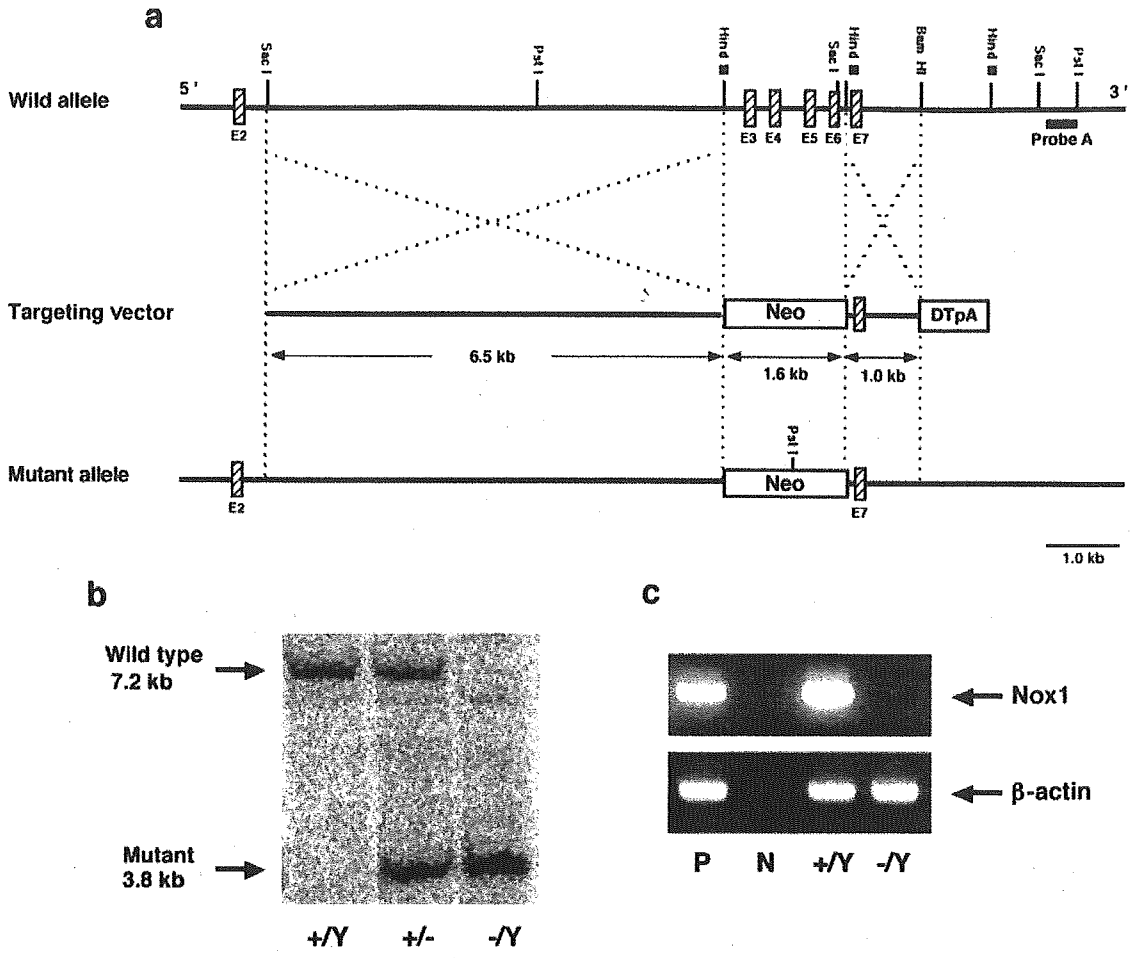

Figure 1. Targeted disruption of the mouse Nox1 gene. a, Diagram of the targeting vector (middle) designed to replace the *Hin*dIII fragment containing exon 3 to exon 6 of the Nox1 gene in the wild-type allele (top) with a pGK-neo cassette (Neo). The predicted mutant allele generated by homologous recombination is shown (bottom). b, Southern blot analysis to verify the homologous recombination. The genomic DNAs obtained from F2 offspring (+/Y, wild-type; +/−, hetero; −/Y, knockout) were digested with *Pst*I and hybridized with probe A, marked as a solid bar in a, located downstream of the targeted region. Bands corresponding to the wild-type allele (7.2 kb) and mutant allele (3.8 kb) are indicated. c, Reverse transcription–PCR of Nox1 mRNA in the colon. Ethidium bromide staining of the products corresponding to the Nox1 transcript (top) and β-actin (bottom). P indicates positive control (mouse colon); N, negative control (no template).

with norepinephrine (30 nmol/L, Sankyo Co). At the maximal constriction level, acetylcholine (ACh, Daiichi Pharmaceutical Co) or sodium pentacyanonitrosylferrate dihydrate (Nacalai Tesque, Kyoto, Japan) was added to evaluate vasodilator function. After a stable relaxation was achieved with ACh, papaverine (100 μmol/L, Sanko Seiyaku Kogyo Co) was added to induce a maximal relaxation. Relaxation was assessed by percent relaxation relative to papaverine-mediated relaxation (100%).

Statistics

The results are expressed as the mean±SEM. For multiple treatment groups, repeated-measures, 2-way, or Latin-square design ANOVA followed by a Tukey-Kramer test was applied. For expression levels of Nox isoforms, a Kruskal-Wallis test was performed, followed by a Dunnett test.

Results

Generation of Nox1-Deficient Mice

Nox1-deficient mice were generated by replacing exon 3 to 6 containing presumed membrane-spanning regions with the neo cassette (Figure 1a). Two independent ES clones yielded germ-line chimeras and their heterozygous mutant F1 mice. Because the locus of the Nox1 gene is on the X chromosome, heterozygotes obtained at F1 generation were female. The heterozygous females were crossed with C57BL/6 males to obtain Nox1-deficient ($^{-/Y}$) mice. The ratio of genotypes of the offspring did not deviate significantly from the expected 1:1 distribution of male Nox1$^{+/Y}$ and Nox1$^{-/Y}$ offspring. Southern blot analysis of the *Pst*I-digested genomic DNA obtained from F2 offspring demonstrated a 7.2-kb band for the wild-type allele and a 3.8-kb band for the mutant allele (Figure 1b). Because mouse Nox1 mRNA is most abundantly expressed in the colon,[5] we verified the expression of Nox1 mRNA in the colon. Although a 902-base band was clearly detected in Nox1$^{+/Y}$ by reverse transcription–PCR, Nox1 mRNA was absent in Nox1$^{-/Y}$ (Figure 1c). Compared with their control littermates, Nox1$^{-/Y}$ grew with normal weight gain and without obvious abnormalities in their general appearance.

Ang II–Induced Superoxide Production Was Reduced in Nox1-Deficient Mice

The effect of Nox1 gene disruption on vascular superoxide production was first investigated by DHE staining of the frozen

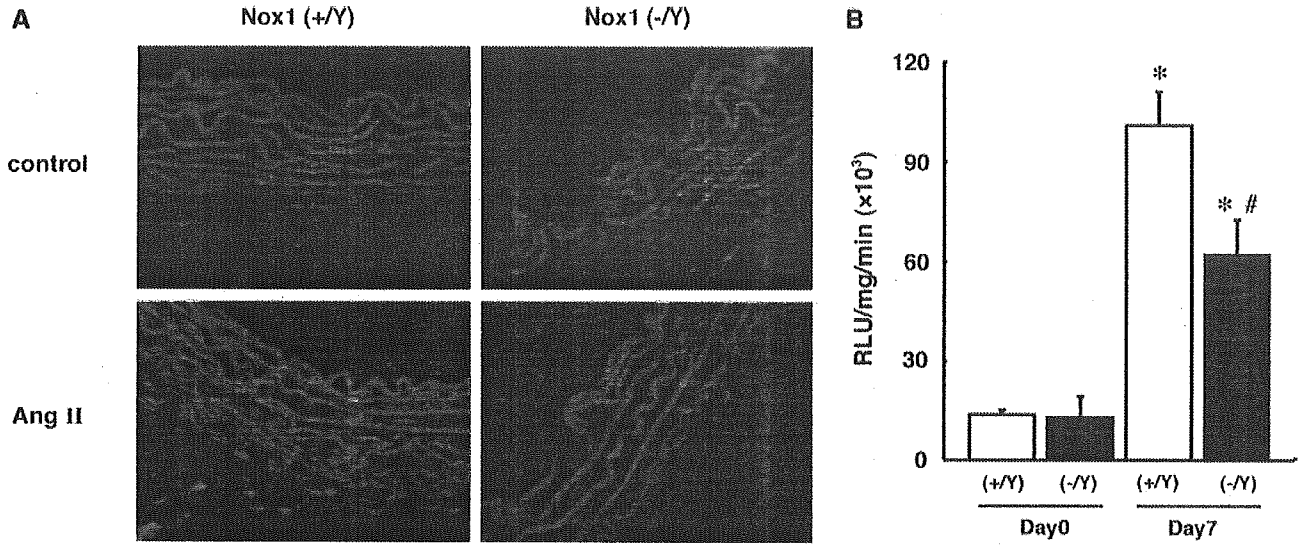

Figure 2. Superoxide production in the thoracic aorta of mice infused with Ang II. A, In situ detection of superoxide production with dihydroethidium (DHE). Cross sections of the thoracic aorta were obtained from mice infused with Ang II (0.7 mg · kg^{-1} · d^{-1}) or vehicle for 7 days. Each image is representative of the results from 3 animals. B, Levels of superoxide in thoracic aortae of mice infused with Ang II or vehicle for 7 days were determined by L-012 chemiluminescence. N=3 to 4 per group. *P<0.05 vs corresponding day 0 group. #P<0.05 vs corresponding $Nox1^{+/Y}$.

sections of the aorta (Figure 2A). A low level of DHE fluorescence was detected in the thoracic aorta of $Nox1^{+/Y}$ or $Nox1^{-/Y}$ after PBS infusion for 7 days. Infusion of Ang II for 7 days markedly increased DHE fluorescence in $Nox1^{+/Y}$ aorta throughout the vessel wall. Conversely, DHE fluorescence in Ang II–treated $Nox1^{-/Y}$ was significantly attenuated in the media.

We next performed the L-012 chemiluminescence assay. No difference in L-012 chemiluminescence was detected in the thoracic aorta of $Nox1^{+/Y}$ or $Nox1^{-/Y}$ after the infusion of PBS for 7 days. In Ang II–infused mice, the chemiluminescence of the aorta was significantly less intense in $Nox1^{-/Y}$ than $Nox1^{+/Y}$ (Figure 2B).

Pressor Response to Ang II Was Suppressed in Nox1-Deficient Mice

Between the age-matched $Nox1^{+/Y}$ and $Nox1^{-/Y}$ mice, no difference in initial body weight was observed. There was no difference in the baseline MBP determined between these experimental groups. In response to continuous infusion of 0.7 mg · kg^{-1} · d^{-1} of Ang II, MBP levels were similarly elevated in both $Nox1^{+/Y}$ and $Nox1^{-/Y}$ until day 5 of treatment. On day 7 of the infusion, however, the increase was significantly suppressed, and a lower MBP was demonstrated in $Nox1^{-/Y}$ compared with $Nox1^{+/Y}$ until day 14 of infusion (Figure 3). Conversely, there was no difference in the basal heart rate between $Nox1^{+/Y}$ and $Nox1^{-/Y}$ (+/Y, 605.3±24.8 versus −/Y, 602.0±25.1 bpm, N=8 to 9). No difference in heart rate of Ang II–infused mice was observed between these groups on day 14 (+/Y, 598.2±18.8 versus −/Y, 599.0±22.0, N=8 to 9).

Ang II–Upregulated Expression of Nox Isoforms in the Aorta

The Ang II–induced elevation in MBP was blunted in $Nox1^{-/Y}$ at 7 days of treatment. We therefore investigated expression levels of Nox1, Nox2, and Nox4 mRNA in the thoracic aorta of mice treated with Ang II. As shown in Figure 4a, Nox1 mRNA levels in $Nox1^{+/Y}$ significantly increased on day 7, and increased levels were sustained during the course of Ang II infusion. A concomitant increase in Nox2 mRNA level was demonstrated on day 5, which returned to the basal level on day 14 (Figure 4b). Conversely, increased Nox4 mRNA levels were observed on days 7 and 14 of Ang II infusion (Figure 4c). In $Nox1^{-/Y}$ mice, similar increases in Nox2 and Nox4 mRNAs were demonstrated at 0, 7, and 14 days of treatment (Figure 4d).

Nox1 Was Not Involved in the Ang II–Induced Vascular Hypertrophy

We previously reported the involvement of Nox1 in prostaglandin $F_{2\alpha}$ ($PGF_{2\alpha}$)–induced hypertrophy of VSMCs in culture.[22] Because vascular hypertrophy is closely linked to elevated blood pressure, we investigated the effect of Ang II

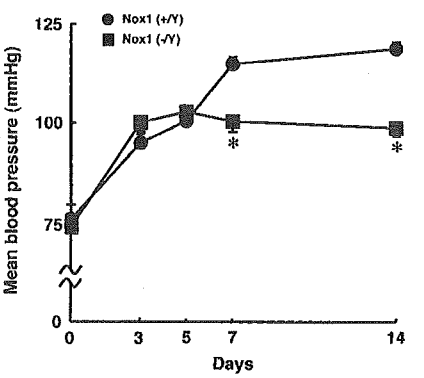

Figure 3. Changes in blood pressure during Ang II infusion. MBP was determined with the tail-cuff system as described in Methods. Ang II was continuously infused with an osmotic pump. N=8 to 9 per group. *P<0.05 vs corresponding $Nox1^{+/Y}$.

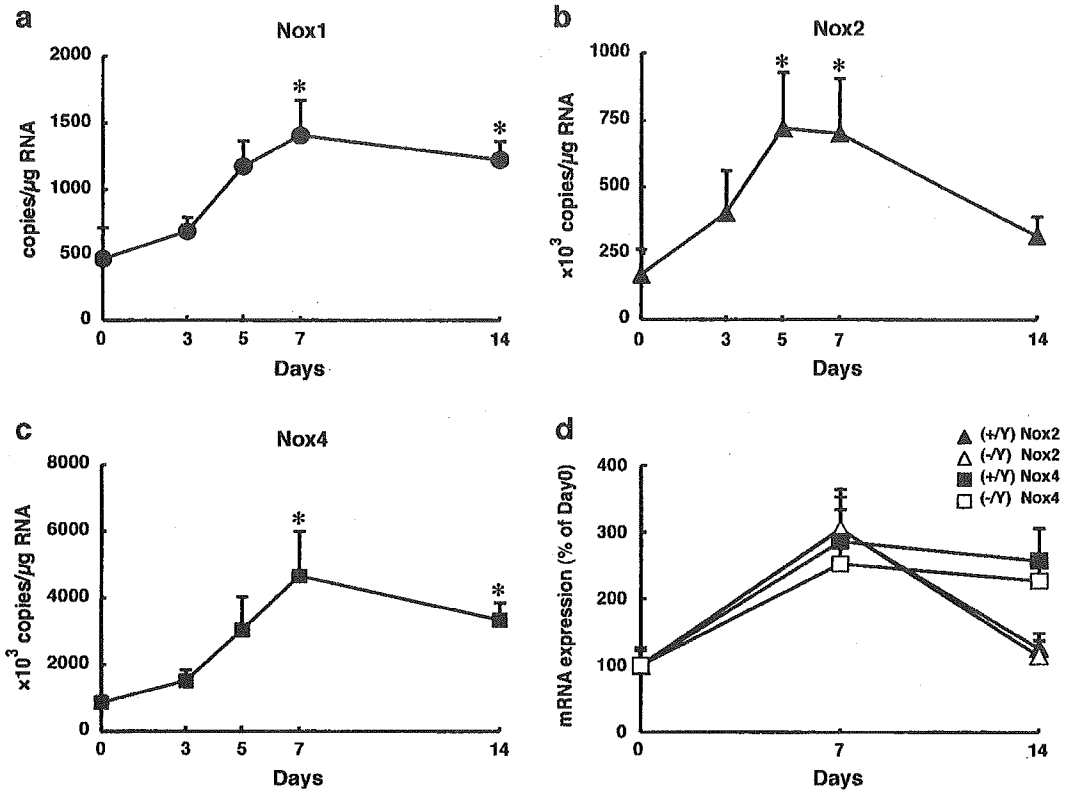

Figure 4. Expression of Nox1 and other Nox isoforms during Ang II infusion. a–c, Time course of expression of Nox isoforms in Nox1$^{+/Y}$. Total RNA was isolated from the thoracic aorta at the indicated day of Ang II infusion. Nox1, Nox2, and Nox4 mRNAs were detected by real-time PCR. Data are expressed as copies per microgram RNA. N=5 per group. *P<0.05 vs day 0. d, Relative mRNA levels of Nox isoforms in Nox1$^{+/Y}$ and Nox1$^{-/Y}$. Data are expressed as levels relative to day 0 (%). N=5 to 7 per group.

infusion on the vascular architecture in Nox1$^{-/Y}$. When medial area and thickness in cross sections of the thoracic aorta were compared, the infusion of Ang II for 14 days was found to have induced significant hypertrophy in both Nox1$^{+/Y}$ and Nox1$^{-/Y}$ (Figure 5a). Contrary to the results of in vitro studies, medial area and thickness of Nox1$^{-/Y}$ were markedly increased, similar to those of Nox1$^{+/Y}$ (Figure 5b). No change in these parameters was observed in control mice infused with vehicle (PBS) for 14 days.

We further investigated the effect of a subpressor dose of Ang II (0.14 mg · kg^{-1} · d^{-1}) in Nox1-deficient mice. As shown in Figure 5c, no change in MBP was observed in mice infused with a subpressor dose of Ang II for 28 days. Under equivalent blood pressure conditions, significant hypertrophy in the media was observed in both Nox1$^{+/Y}$ and Nox1$^{-/Y}$. Medial area and thickness of the thoracic aorta increased in Nox1$^{-/Y}$ to an extent similar to that in Nox1$^{+/Y}$.

L-NAME Abolished the Suppression of Pressor Response to Ang II in Nox1-Deficient Mice

In Ang II–induced hypertension, superoxide derived from vascular NADPH oxidase has been reported to impair endothelium-dependent relaxation by inactivating nitric oxide (NO), an endothelial vasodilator. To investigate the possible interaction between Nox1 deficiency and endogenous NO, we administered 1.4 mg/d of L-NAME, an NO synthase inhibitor, to Nox1$^{+/Y}$ and Nox1$^{-/Y}$ (Figure 6A). Administration of L-NAME for 14 days slightly elevated basal MBP levels in Nox1$^{+/Y}$ and Nox1$^{-/Y}$, although the effect was statistically insignificant. The pressor response to Ang II in Nox1$^{+/Y}$ was unaffected by L-NAME, whereas in Ang II–infused Nox1$^{-/Y}$, MBP was significantly elevated by administration of L-NAME. Consequently, no difference in MBP levels was observed between Nox1$^{+/Y}$ and Nox1$^{-/Y}$ treated with Ang II along with L-NAME.

cGMP Level in the Aorta Was Preserved in Nox1-Deficient Mice Infused With Ang II

To evaluate the effect of disruption of Nox1/NADPH oxidase on NO bioactivity, we measured the level of cGMP in the thoracic aorta. As shown in Figure 6B, no difference in cGMP levels was observed between Nox1$^{+/Y}$ and Nox1$^{-/Y}$ infused with vehicle (PBS) for 7 days. In Ang II–infused mice, conversely, cGMP levels were significantly decreased in Nox1$^{+/Y}$, whereas the levels in Nox1$^{-/Y}$ were retained. No difference in the activity of NO synthase was demonstrated between Nox1$^{+/Y}$ and Nox1$^{-/Y}$ treated with Ang II (data not shown).

Endothelium-Dependent Vasodilatation Was Preserved in Nox1-Deficient Mice Infused With Ang II

Finally, vascular relaxations in aortic strips were studied to determine whether Nox1-derived ROSs are involved in the

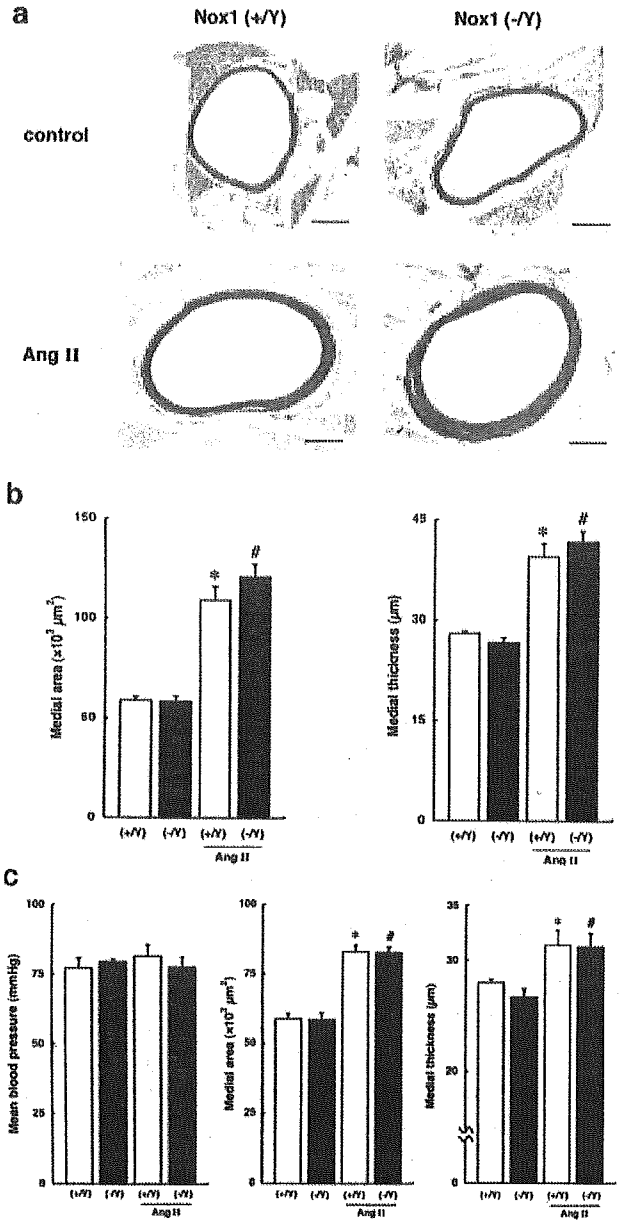

Figure 5. Histological analysis of the thoracic aorta of mice infused with Ang II. a, Representative cross sections of the thoracic aorta stained with elastica van Gieson stain. Scale bar=200 μm. b, Quantitative analyses of medial area (left) and thickness (right). Ang II (0.7 mg · kg^{-1} · d^{-1}) or vehicle was infused for 14 days. N=5 to 6 per group. *P<0.05, #P<0.05 vs corresponding vehicle-treated group. c, Effects of a subpressor dose of Ang II infusion. Ang II (0.14 mg · kg^{-1} · d^{-1}) or vehicle was continuously infused with an osmotic pump for 28 days, when MBP (left), medial area (middle), and thickness (right) were determined. N=5 to 6 per group. *P<0.05, #P<0.05 vs corresponding vehicle-treated group.

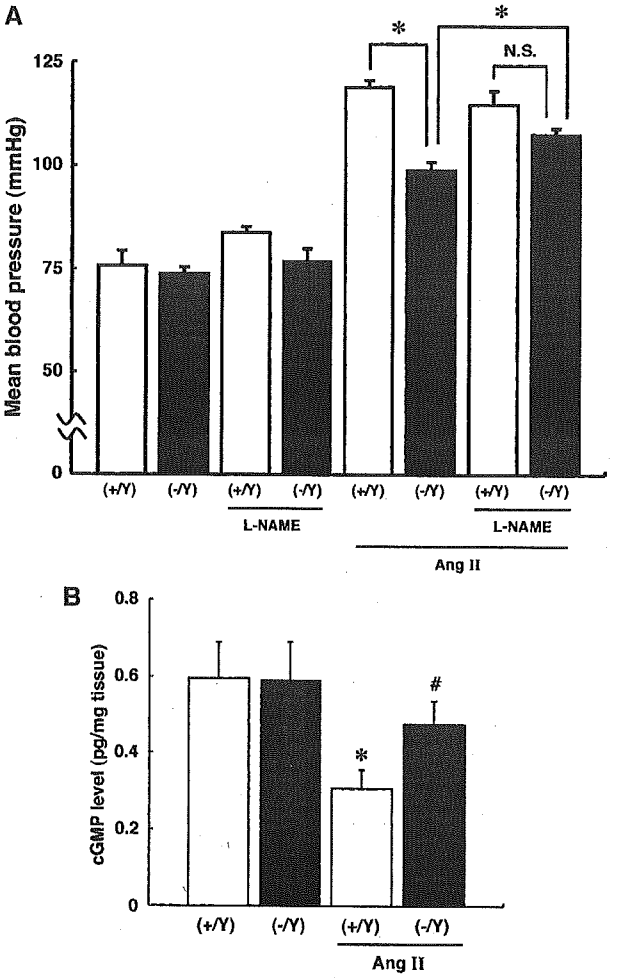

Figure 6. NO signaling in Ang II–infused mice. A, Effects of L-NAME on pressor response to Ang II. Reduced pressor response to Ang II in Nox1$^{-/Y}$ was abolished by administration of L-NAME (1.4 mg/d). MBP was determined on day 14 of vehicle or Ang II infusion. N=5 to 9 per group. *P<0.05; N.S., not significant. B, Aortic cGMP level. cGMP levels in thoracic aortae of mice infused with Ang II or vehicle for 7 days were measured by an enzyme immunoassay. N=7 to 11 per group. *P<0.05 vs vehicle-treated Nox1$^{+/Y}$. #P<0.05 vs Ang II–infused Nox1$^{+/Y}$.

Ang II–induced alteration in vascular reactivity. In the vehicle-infused Nox1$^{-/Y}$, the response to ACh was slightly better than that in Nox1$^{+/Y}$, without statistical significance (Figure 7a). After the infusion of Ang II for 7 days, the response to ACh was significantly attenuated in Nox1$^{+/Y}$. In contrast, Ang II infusion did not affect the ACh-induced relaxation in Nox1$^{-/Y}$. As shown in Figure 7b, endothelium-independent relaxations to sodium pentacyanonitrosylferrate dihydrate were similar in aortic strips obtained from all experimental groups. Usage of $PGF_{2\alpha}$ as an alternative contractile substance gave similar results, and no difference in the contractile response to norepinephrine or Ang II was observed between Nox1$^{+/Y}$ and Nox1$^{-/Y}$ infused with vehicle or Ang II (data not shown). These findings suggest that scavenging of NO by Nox1-derived ROSs underlies the development of Ang II–induced hypertension.

Discussion

In this study, we clarified for the first time the role of Nox1 in the pathogenesis of Ang II–mediated hypertension using Nox1-deficient mice. The principal findings obtained were that ROSs derived from Nox1/NADPH oxidase are crucial to

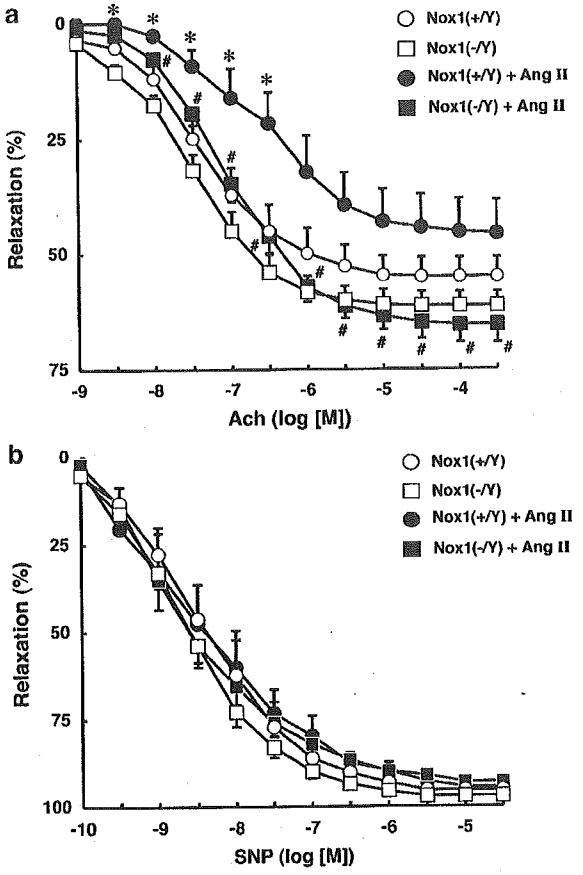

Figure 7. Vascular relaxations in Ang II–infused mice. After the infusion of vehicle or Ang II for 7 days, vascular reactivity to endothelium-dependent agonist ACh (a) or endothelium-independent NO donor sodium pentacyanonitrosylferrate dihydrate (SNP) (b) was measured in isolated aortic strips. N=4 to 6 per group. *$P<0.05$ vs vehicle-treated Nox1$^{+/Y}$. #$P<0.05$ vs Ang II–infused Nox1$^{+/Y}$.

the pressor response to Ang II by reducing the bioavailability of NO.

The present findings suggest that Nox1 is involved in the late phase but not in the early phase of the pressor response to Ang II. In both Nox1$^{+/Y}$ and Nox1$^{-/Y}$, MBP was increased up to day 5 of Ang II infusion, whereas in Nox1$^{-/Y}$, the pressor response was blunted after 7 days. Meanwhile, Nox1 mRNA expression was markedly upregulated from day 7 in Nox1$^{+/Y}$. Vascular superoxide production is known to impair vascular relaxation through the inactivation of endothelial NO, which serves as an important component in the development and maintenance of increased blood pressure.[23] It has been reported that administration of tempol, a superoxide dismutase mimetic, abolishes the pressor response to Ang II.[24] We also observed that administration of tempol almost completely abolished the pressor response to Ang II in both Nox1$^{+/Y}$ and Nox1$^{-/Y}$ (data not shown). It therefore seems likely that ROSs derived from another source participate in the early phase of the pressor response to Ang II. In the present Ang II–treated mice, a marked increase in Nox2 mRNA in the aorta was demonstrated at day 5 and 7. In a previous study using Nox2-deficient mice, however, infusion of Ang II for 6 days caused an increase in systolic blood pressure similar to that in wild-type mice.[14] A recent study also reported that inactivation of Nox2 had no effect on the development of hypertension in a model in which the endogenous renin-angiotensin system is chronically upregulated.[15] These findings therefore suggest that Nox2 does not participate in the late phase of the hypertensive response to Ang II in a murine animal model. Meanwhile, a gradual increase in Nox4 mRNA was observed during Ang II infusion, but the level was unchanged at day 3, when the early phase of the pressor response was already depicted. Although the source of ROSs responsible for the early phase of increased MBP in Ang II–infused Nox1$^{-/Y}$ is still unclear, an alternative possibility may be that a rapid increase in superoxide production by activated Nox2 or Nox4/NADPH oxidase takes part in the early phase of the hypertensive response in Nox1$^{-/Y}$. Ang II–induced production of ROSs by NADPH oxidase is known to take place instantly, which depends on the activation of protein kinase C and a small G protein, Rac.[25]

Ang II induces vascular hypertrophy, and it is well known that vascular hypertrophy is closely linked to elevation in blood pressure. We previously demonstrated that depletion of Nox1 mRNA by ribozymes significantly reduced the increased protein synthesis induced by $PGF_{2\alpha}$ in a rat VSMC-derived cell line.[22] Nox1 in fact mediates Ang II–induced activation of the redox-sensitive signaling molecules, p38 mitogen-activated protein kinase and Akt, both of which are required for hypertrophy of VSMCs.[12] However, our study demonstrated that hypertrophic responses to pressor and subpressor doses of Ang II in Nox1$^{-/Y}$ were similar to those in Nox1$^{+/Y}$. These findings clearly indicate that Nox1 is not associated with the development of vascular hypertrophy induced by Ang II, which is inconsistent with the previous studies in vitro. Why such inconsistent findings have come about is a subject for further investigation. Under conditions in vivo, however, the ROSs responsible for vascular hypertrophy may derive primarily from Nox2 localized in the endothelial and adventitial cells. ROSs derived from Nox1 may have a limited effect because of its low level of activity compared with that of Nox2.[4] Because such growth-promoting ROSs as hydrogen peroxide diffuse freely across the cell membrane, VSMCs in Ang II–infused Nox1$^{-/Y}$ may yet be exposed to a high level of ambient ROSs, whereas isolated VSMCs in culture are unaffected by Nox2-derived ROSs. Also to be considered is the fact that VSMCs removed from their tissue of origin and placed in cell culture transform from a contractile to a synthetic phenotype.[26] In vascular injury and atherosclerosis, VSMCs also transform from a contractile to a synthetic phenotype.[27,28] Although hypertrophy in the aorta of Ang II–infused mice developed in the absence of Nox1, the findings in cell culture suggest that Nox1 may be involved in vascular remodeling under different experimental or pathological conditions.

Administration of L-NAME abolished the effect of Nox1 gene disruption on the pressor response to Ang II, whereas the level of cGMP, a second messenger of the NO signaling cascade, was preserved in Ang II–infused Nox1$^{-/Y}$ vessels. It

has been generally accepted that ROSs decrease the bioavailability of NO by scavenging NO and causing endothelial NO synthase uncoupling, thereby contributing to the pathogenesis of hypertension.[29] Uncoupling of endothelial NO synthase appears not to be involved in the pressor response to Ang II under our experimental conditions, because pretreatment with L-NAME did not affect superoxide production in aortic rings isolated from Ang II–treated mice (data not shown). Our findings thus suggest that the preservation of the availability of NO through depletion of Nox1-derived ROSs is the underlying mechanism of the suppressed pressor response in Nox1$^{-/Y}$. The fact that endothelium-dependent vascular relaxation was maintained in Ang II–infused Nox1$^{-/Y}$ aorta further strengthens this view.

It should be noted that Nox1-derived ROSs participated primarily in the pressor response to Ang II, although an Ang II–induced increase in superoxide production could be attributed to augmented expression of Nox2 and Nox4 in the vascular wall as well. In the thoracic aorta, quantitative determination of mRNA levels illustrated dominant expression of Nox2 and Nox4 compared with Nox1. However, superoxide production in isolated aorta was significantly attenuated in Ang II–infused Nox1$^{-/Y}$. Such a discrepancy in the levels of Nox transcripts expressed in the aorta and their relative contribution to superoxide production may be explained by distribution and interaction of these catalytic subunits with other subunits required for full enzyme activity.[23] ROSs generated by NADPH oxidase act as intracellular and intercellular signaling molecules,[12] and Nox1-derived ROSs in the kidney may also participate in the regulation of the pressor response to Ang II.[30] In this context, multiple sites of action may be involved in the antihypertensive response in Nox1$^{-/Y}$.

To date, no isoform-specific inhibitors of the Nox family have been developed. Knockout mice are therefore important tools with which to clarify the functional roles of Nox isoforms in vivo. A previous report using Nox2-deficient mice demonstrated the involvement of Nox2 in the regulation of the basal blood pressure and in Ang II–induced vascular hypertrophy but not in the pressor response to Ang II.[14,15] Taking these findings into consideration, it is notable that each Nox isoform plays a distinct role in the development of vascular disorders. Isoform-specific inhibitors of the Nox family may therefore become ideal therapeutic agents for the treatment of vascular disorders with diverse pathological backgrounds.

Acknowledgments

We thank Dr N. Urao of the Department of Cardiovascular Medicine and Drs T. Nishinaka, M. Ibi, and N. Arakawa of the Department of Pharmacology for valuable discussion and advice. We are also grateful to Drs T. Aihara, K. Amagase, and E. Nakamura of the Department of Applied Pharmacology, Kyoto Pharmaceutical University, for valuable advice and assistance. The authors are indebted to Dr J. Takeda of the Department of Social and Environmental Medicine, Osaka University, for initial guidance with the gene targeting study. This work was supported in part by a Grant-in-Aid for Young Scientists (B) 16790310 (to K. Iwata) and 14770036 (to Dr Katsuyama) from the Ministry of Education, Culture, Sports, Science, and Technology of Japan.

References

1. Kim S, Iwao H. Molecular and cellular mechanisms of angiotensin II-mediated cardiovascular and renal diseases. *Pharmacol Rev.* 2000;52:11–34.
2. Griendling KK, Minieri CA, Ollerenshaw JD, Alexander RW. Angiotensin II stimulates NADH and NADPH oxidase activity in cultured vascular smooth muscle cells. *Circ Res.* 1994;74:1141–1148.
3. Zhang H, Schmeisser A, Garlichs CD, Plotze K, Damme U, Mugge A, Daniel WG. Angiotensin II–induced superoxide anion generation in human vascular endothelial cells: role of membrane-bound NADH-/NADPH-oxidases. *Cardiovasc Res.* 1999;44:215–222.
4. Griendling KK, Sorescu D, Ushio-Fukai M. NAD(P)H oxidase: role in cardiovascular biology and disease. *Circ Res.* 2000;86:494–501.
5. Suh YA, Arnold RS, Lassegue B, Shi J, Xu X, Sorescu D, Chung AB, Griendling KK, Lambeth JD. Cell transformation by the superoxide-generating oxidase Mox1. *Nature.* 1999;401:79–82.
6. Lambeth JD. NOX enzymes and the biology of reactive oxygen. *Nat Rev Immunol.* 2004;4:181–189.
7. Ago T, Kitazono T, Ooboshi H, Iyama T, Han YH, Takada J, Wakisaka M, Ibayashi S, Utsumi H, Iida M. Nox4 as the major catalytic component of an endothelial NAD(P)H oxidase. *Circulation.* 2004;109:227–233.
8. Gorlach A, Brandes RP, Nguyen K, Amidi M, Dehghani F, Busse R. A gp91phox containing NADPH oxidase selectively expressed in endothelial cells is a major source of oxygen radical generation in the arterial wall. *Circ Res.* 2000;87:26–32.
9. Pagano PJ, Clark JK, Cifuentes-Pagano ME, Clark SM, Callis GM, Quinn MT. Localization of a constitutively active, phagocyte-like NADPH oxidase in rabbit aortic adventitia: enhancement by angiotensin II. *Proc Natl Acad Sci U S A.* 1997;94:14483–14488.
10. Sorescu GP, Song H, Tressel SL, Hwang J, Dikalov S, Smith DA, Boyd NL, Platt MO, Lassegue B, Griendling KK, Jo H. Bone morphogenic protein 4 produced in endothelial cells by oscillatory shear stress induces monocyte adhesion by stimulating reactive oxygen species production from a nox1-based NADPH oxidase. *Circ Res.* 2004;95:773–779.
11. Szocs K, Lassegue B, Sorescu D, Hilenski LL, Valppu L, Couse TL, Wilcox JN, Quinn MT, Lambeth JD, Griendling KK. Upregulation of Nox-based NAD(P)H oxidases in restenosis after carotid injury. *Arterioscler Thromb Vasc Biol.* 2002;22:21–27.
12. Lassegue B, Sorescu D, Szocs K, Yin Q, Akers M, Zhang Y, Grant SL, Lambeth JD, Griendling KK. Novel gp91(phox) homologues in vascular smooth muscle cells: nox1 mediates angiotensin II–induced superoxide formation and redox-sensitive signaling pathways. *Circ Res.* 2001;88:888–894.
13. Mollnau H, Wendt M, Szocs K, Lassegue B, Schulz E, Oelze M, Li H, Bodenschatz M, August M, Kleschyov AL, Tsilimingas N, Walter U, Forstermann U, Meinertz T, Griendling K, Munzel T. Effects of angiotensin II infusion on the expression and function of NAD(P)H oxidase and components of nitric oxide/cGMP signaling. *Circ Res.* 2002;90:E58–E65.
14. Wang HD, Xu S, Johns DG, Du Y, Quinn MT, Cayatte AJ, Cohen RA. Role of NADPH oxidase in the vascular hypertrophic and oxidative stress response to angiotensin II in mice. *Circ Res.* 2001;88:947–953.
15. Touyz RM, Mercure C, He Y, Javeshghani D, Yao G, Callera GE, Yogi A, Lochard N, Reudelhuber TL. Angiotensin II-dependent chronic hypertension and cardiac hypertrophy are unaffected by gp91phox-containing NADPH oxidase. *Hypertension.* 2005;45:530–537.
16. Landmesser U, Cai H, Dikalov S, McCann L, Hwang J, Jo H, Holland SM, Harrison DG. Role of p47(phox) in vascular oxidative stress and hypertension caused by angiotensin II. *Hypertension.* 2002;40:511–515.
17. Takeya R, Ueno N, Kami K, Taura M, Kohjima M, Izaki T, Nunoi H, Sumimoto H. Novel human homologues of p47phox and p67phox participate in activation of superoxide-producing NADPH oxidases. *J Biol Chem.* 2003;278:25234–25246.
18. Wood SA, Pascoe WS, Schmidt C, Kemler R, Evans MJ, Allen ND. Simple and efficient production of embryonic stem cell-embryo chimeras by coculture. *Proc Natl Acad Sci U S A.* 1993;90:4582–4585.
19. Wassmann S, Stumpf M, Strehlow K, Schmid A, Schieffer B, Bohm M, Nickenig G. Interleukin-6 induces oxidative stress and endothelial dysfunction by overexpression of the angiotensin II type 1 receptor. *Circ Res.* 2004;94:534–541.
20. Daiber A, August M, Baldus S, Wendt M, Oelze M, Sydow K, Kleschyov AL, Munzel T. Measurement of NAD(P)H oxidase-derived superoxide with the luminol analogue L-012. *Free Radic Biol Med.* 2004;36:101–111.

21. Fujiyama S, Amano K, Uehira K, Yoshida M, Nishiwaki Y, Nozawa Y, Jin D, Takai S, Miyazaki M, Egashira K, Imada T, Iwasaka T, Matsubara H. Bone marrow monocyte lineage cells adhere on injured endothelium in a monocyte chemoattractant protein-1–dependent manner and accelerate reendothelialization as endothelial progenitor cells. *Circ Res.* 2003;93:980–989.
22. Katsuyama M, Fan C, Yabe-Nishimura C. NADPH oxidase is involved in prostaglandin F2alpha-induced hypertrophy of vascular smooth muscle cells: induction of NOX1 by PGF2alpha. *J Biol Chem.* 2002;277:13438–13442.
23. Lassegue B, Clempus RE. Vascular NAD(P)H oxidases: specific features, expression, and regulation. *Am J Physiol.* 2003;285:R277–R297.
24. Ortiz MC, Manriquez MC, Romero JC, Juncos LA. Antioxidants block angiotensin II–induced increases in blood pressure and endothelin. *Hypertension.* 2001;38:655–659.
25. Seshiah PN, Weber DS, Rocic P, Valppu L, Taniyama Y, Griendling KK. Angiotensin II stimulation of NAD(P)H oxidase activity: upstream mediators. *Circ Res.* 2002;91:406–413.
26. Chamley-Campbell J, Campbell GR, Ross R. The smooth muscle cell in culture. *Physiol Rev.* 1979;59:1–61.
27. Lusis AJ. *Atherosclerosis Nature.* 2000;407:233–241.
28. Owens GK. Regulation of differentiation of vascular smooth muscle cells. *Physiol Rev.* 1995;75:487–517.
29. Cai H, Harrison DG. Endothelial dysfunction in cardiovascular diseases: the role of oxidant stress. *Circ Res.* 2000;87:840–844.
30. Chabrashvili T, Kitiyakara C, Blau J, Karber A, Aslam S, Welch WJ, Wilcox CS. Effects of ANG II type 1 and 2 receptors on oxidative stress, renal NADPH oxidase, and SOD expression. *Am J Physiol.* 2003;285:R117–R124.

CLINICAL PERSPECTIVE

Involvement of reactive oxygen species (ROSs) generated by membrane-bound NADPH oxidase has been suggested in the pathogenesis of various cardiovascular diseases. NADPH oxidase is a multisubunit enzyme comprising a membrane-associated catalytic subunit (Nox) and several cytosolic regulatory subunits. Among the Nox isoforms recently identified, vascular Nox1 is detected in smooth muscle cells and endothelial cells, whereas Nox2 is localized in endothelial and adventitial cells. A previous report using Nox2-deficient mice demonstrated the involvement of Nox2 in the regulation of the basal blood pressure and in Ang II–induced vascular hypertrophy, but not in the pressor response to Ang II. In this study, Nox1-deficient mice were generated and chronically infused with Ang II. The elevation of blood pressure was significantly blunted compared with wild-type mice, whereas the infusion of pressor as well as subpressor doses of Ang II did elicit marked hypertrophy in the Nox1-deficient aorta. The underlying mechanism of the suppressed pressor response to Ang II was indicated to be the preservation of the availability of nitric oxide through depletion of Nox1-derived ROSs. Nox1/NADPH oxidase, as a downstream unit of Ang II, thus plays a major role in renin-angiotensin system–mediated chronic hypertension. Certainly, roles for NADPH oxidase in ischemic heart disease, cardiac hypertrophy, and arteriosclerosis should be further clarified in Nox-deficient mice. Because each Nox isoform appears to play a distinct role in the development of vascular disorders, isoform-specific inhibitors of the Nox family may become a new generation of therapeutic agents for the treatment of cardiovascular diseases with diverse pathological backgrounds.

Available online at www.sciencedirect.com
SCIENCE DIRECT®
ELSEVIER
Biochemical and Biophysical Research Communications 336 (2005) 118–127
BBRC
www.elsevier.com/locate/ybbrc

Sonoporation using microbubble BR14 promotes pDNA/siRNA transduction to murine heart

Sei Tsunoda [a,b,c], Osam Mazda [c,*], Yohei Oda [a,b], Yasunori Iida [a,b,c], Satoshi Akabame [a,b], Tsunao Kishida [c], Masaharu Shin-Ya [c], Hidetsugu Asada [c], Satoshi Gojo [d], Jiro Imanishi [c], Hiroaki Matsubara [a], Toshikazu Yoshikawa [b]

[a] *Department of Molecular Cardiology and Vascular Regenerative Medicine, Graduate School of Medical Science, Kyoto Prefectural University of Medicine, Kyoto 602-8566, Japan*
[b] *Department of Inflammation and Immunology, Graduate School of Medical Science, Kyoto Prefectural University of Medicine, Kyoto 602-8566, Japan*
[c] *Department of Microbiology, Graduate School of Medical Science, Kyoto Prefectural University of Medicine, Kyoto 602-8566, Japan*
[d] *Department of Cardiovascular Surgery, Saitama Medical Center, Kawagoe, Saitama 350-8550, Japan*

Received 28 July 2005
Available online 18 August 2005

Abstract

Naked plasmid DNA (pDNA) and short interfering RNA (siRNA) duplexes were transduced into adult murine heart by means of sonoporation using the third-generation microbubble, BR14. Plasmid DNAs carrying luciferase, β-galactosidase (β-gal), or enhanced green fluorescent protein (EGFP) reporter genes were mixed with BR14 and injected percutaneously into the left ventricular (LV) cavity of C57BL/6 mice while exposed to transthoracic ultrasound at 1 MHz for 60 s. Sonoporation at an output intensity of 2.0 W/cm^2 and a 50% pulse duty ratio resulted in the highest luciferase expression in the heart. Histological examinations revealed significant expression of the β-gal and EGFP reporters in the subendocardial myocardium of LV. Intraventricular co-injection of siRNA-GFP and BR14 with concomitant ultrasonic exposure resulted in substantial reduction in EGFP expression in the coronary artery in EGFP transgenic mice. The present method may be applicable to gain-of-function and loss-of-function genetic engineering in vivo of adult murine heart.
© 2005 Elsevier Inc. All rights reserved.

Keywords: Naked plasmid DNA; Heart; Sonoporation; Microbubble; Gene transfer; RNA interference; Ultrasound; Gene therapy; Molecular therapy

Genetic modification of the heart may provide a powerful molecular tool for improving our understanding of cardiac diseases. Moreover, a technology that enables safe and efficient gene delivery to the heart may provide a novel therapeutic modality to control heart disorders. Some studies recently demonstrated that efficient transfer of genes into murine heart can be achieved by intracoronary infusion of adenoviral or adeno-associated viral vectors followed by transient aortic occlusion [1,2]. Viral vector-mediated procedures, however, may induce complications associated with recombinant viruses, hindering clinical application of the systems to gene therapy for cardiovascular diseases. Although non-viral methods are free from virus-associated adverse effects, their transduction efficiency is low. For example, following direct intramyocardial injection of plasmid DNA into the heart of mice [3], rats [4,5], and hamsters [6], the transgenes were expressed only within a small area surrounding the injection site.

* Corresponding author. Fax: +81 75 251 5331.
E-mail address: mazda@koto.kpu-m.ac.jp (O. Mazda).

0006-291X/$ - see front matter © 2005 Elsevier Inc. All rights reserved.
doi:10.1016/j.bbrc.2005.08.052

A more efficient non-viral method of gene transfer is sonoporation of cells. In sonoporation, ultrasound is used to increase the porosity of the cell membrane [7]. The ultrasound induces the formation of cavitation bubbles that by mechanical action cause enough damage to the cell membrane to allow large molecules in the surrounding medium to enter the cell, but not so much damage that the cell cannot reseal the membrane and survive [8]. The extent of cavitation bubble formation and subsequent increase in membrane permeability can be enhanced by use of microbubble echo contrast agents. This method has been applied to skeletal muscle of mice [9], as well as myocardium of both rats [10] and dogs [11], in vivo, using various microbubble agents including Levovist, Hexabrix, and Optison [9–18]. It has been indicated that the transfection efficiency is dependent on both the ultrasound parameters and the formulation of microbubbles.

BR14 (Bracco Research SA, Geneva, Switzerland) is a recently developed ultrasound contrast agent, which has some advantages over other echo contrast agents [19,20], because it consists of stabilized relatively small microbubbles and is transiently retained within capillaries. These qualities mean that BR14 may be a better agent in sonoporation-mediated transfection. Indeed, recent studies have indicated that BR14 effectively enhanced sonoporation-based gene transfection into hepatic cancer implant in mice [21] as well as into saphenous vein graft in porcine [22].

RNA interference (RNAi) is a powerful means of analyzing the function of genes in basic researches, while the technology may also be quite useful in developing therapeutic molecular targeting strategies for treatment of diseases. RNAi was first discovered in the nematode *Caenorhabditis elegans* as a response to double-stranded RNA, which induced sequence-specific silencing of gene expression [23]. In mammalian cells, short interfering RNA (siRNA) 21–23 nucleotide pairs in length silences the gene with the homologous sequence [23,24]. The in vivo effectiveness of siRNA-mediated silencing was also studied in various organs, including the liver [25,26] and the skeletal muscle [27]. However, in vivo RNAi in cardiac tissues has not been reported so far.

In the present study, we investigated whether BR14 facilitates sonoporation-mediated transfection of naked plasmid DNA into the adult murine heart. Moreover, we applied this method to transfer synthetic siRNA duplex, to knock down targeted genes in the heart in vivo.

Materials and methods

Animals. Female C57BL/6 mice (16.8 ± 0.7 weeks old, weighing 24.0 ± 0.5 g) were purchased from Shimizu Laboratory Suppliers (Kyoto, Japan). Enhanced green fluorescent protein (EGFP) transgenic mice (TGM) (27.3 ± 4.8 weeks old, weighing 25.3 ± 1.1 g) were purchased from Charles River Japan (Yokohama, Japan). All the animal experiments were performed according to the approved guidelines of Kyoto Prefectural University of Medicine.

Plasmid vectors and siRNA. The plasmids pGEG.GL3 [28], pGEG.EGFP [29], and pGEG.β [30] carried GL3 firefly luciferase (Luc), EGFP, and *Escherichia coli* β-galactosidase (β-gal) genes, respectively, under the control of the CAG promoter. Each plasmid also contained Epstein–Barr virus (EBV) nuclear antigen 1 (EBNA1) gene and EBV oriP sequence [31]. Plasmids were purified using Qiagen MegaPrep Endo-free kits (Qiagen, Hilden, Germany). siRNA duplex targeting GFP (siRNA-GFP) was purchased from Dharmacon (Lafayette, CO, USA).

In vivo experiments. Plasmid DNA (500 μg) or siRNA (40 μg) was diluted in 400 μl PBS and mixed with 100 μl BR14 microbubble. Mice were anesthetized by an intraperitoneal injection of sodium pentobarbital (40 μg/g body weight), and tracheotomy was performed in the supine position to provide ventilation via a ventilator (MiniVent 845; Hugo Sachs Elektronik, March-Hugstetten, Germany) at the rate of 150 cycles per min. An incision was made in the greater and smaller pectoral muscles, and the microbubble/nucleic acid solution was injected over a period of about 10 s into the left ventricular (LV) cavity via the intercostal muscle using a 27-gauge needle. The same solution was injected into the tail vein (TV) of another group of mice. At the same time as the initiation of the injection, transthoracic ultrasound insonation (sonication) was performed through a 6-mm diameter probe with an input frequency of 1 MHz, an output intensity of 1.0–2.0 W/cm^2, a pulse duty ratio (PDR) of 10–50%, and a duration of 60 s. A Sonitron 2000 (Rich-Mar, Inola, OK, USA) was used to generate the ultrasound. Hydrodynamics-based transduction was performed as described previously [28]. Briefly, 40 μg siRNA-GFP was diluted in 1600 μl PBS and injected intravenously within 4s via the tail vein using a 27-gauge needle.

Echocardiography and ECG monitoring. Transthoracic echocardiography was performed using an ultrasound platform (Nemio 30, Toshiba Medical, Tokyo, Japan) equipped with a 13-MHz imaging transducer. Under anesthesia, a parasternal view was obtained and M-mode images of the LV were recorded. Electrocardiographic monitoring was performed by limb lead (II) during the sonoporation.

Luciferase assay. Biventricular muscle was minced with a pair of scissors and homogenized in 200 μl of reporter lysis buffer (Promega, Madison, WI, USA) using a sonicator. The extract was centrifuged at 14,000*g* for 15 min, and the Luc activity in the supernatant was measured as described [32]. Organs other than the heart were also treated as described above. Protein concentration in the extract was determined as described previously [28].

X-gal staining. The heart was fixed with 4% paraformaldehyde and dehydrated in sucrose solution. The specimens were then stained with X-gal solution (0.05% (v/v) 5-bromo-4-chloro-3-indolyl-β-D-galactoside (X-gal; Nacalai Tesque, Kyoto, Japan), 1 mM $MgCl_2$, 150 mM NaCl, 3 mM $K_4[Fe(CN)_6]$, 3 mM $K_3[Fe(CN)_6]$, 60 mM Na_2HPO_4, 40 mM NaH_2PO_4, and 0.1% Triton X-100). After 12 h of incubation at 37 °C, the reaction was terminated by replacing the solution with PBS [33].

Fluorescence microscopic observation and immunohistochemistry. After perfusion with saline, the heart was fixed with 4% paraformaldehyde and dehydrated in sucrose solution. The specimens were embedded in OCT compound and immediately frozen at −80 °C. Serial sections 10 μm thick were cut on a cryostat and observed under a fluorescence microscope with excitation at 488 nm. The cryosections were stained with anti-GFP antibody (Molecular Probes, Leiden, The Netherlands) and visualized using the avidin/biotin/peroxidase method (Vector Laboratories, Burlingame, CA).

Statistical analysis. Differences among continuous variables were tested by Student's *t* test for paired and unpaired observations and by ANOVA with Fisher's PLSD correction for repeated comparisons. A value of $P < 0.05$ was considered to be statistically significant.

Results

Influence of sonoporation to the heart

A mixture of plasmid DNA and BR14 microbubble was injected into the LV of mice. Echocardiographic examinations were performed before and after the injection. The myocardium and the LV lumen were separated by endocardium that was visible before the treatment (Fig. 1Aa). After BR14 injection, the myocardium and the LV cavity showed comparable echo intensities, and the boundary between them was unclear (Fig. 1Ab). The hearts of the mice were sonicated under several conditions. After continuous sonication at 2.0 W/cm^2 and 50% PDR (2.0 W/50% PDR) for 60 s, most of the BR14 was disrupted, while a few residual circulating microbubbles were seen in the ventricle (Figs. 1Ac and Ad, arrowheads). The echocardiographic appearance subsequently became normal thereafter (data not shown).

Electrocardiographic examination was also performed to assess the influence of sonotransfection on the murine heart. Arrhythmia was seen in the mice exposed to ultrasound at 2.0 W/50% PDR after pDNA and BR14 had been injected into the LV, but they all quickly recovered from the same. Fig. 1B shows representative ECG changes before, during, and after the manipulation. Compared with the ECG profile before sonication (Fig. 1Ba), the QRS complex was prolonged immediately after the initiation of the ultrasound exposure (Fig. 1Bb). Thirty seconds later, the mice showed atrioventricular (AV) block (Fig. 1Bc), which persisted thereafter (Fig. 1Bd). Two minutes after termination of the sonication, the heart rate suddenly recovered to baseline (Figs. 1Be and Bf). In other cases, the AV block continued for shorter periods, ranging from 10 s to 2 min.

Echocardiographic analyses were performed to evaluate the LV contractility before and after sonoporation-mediated transfection (LV method, 2.0 W/50% PDR). As shown in Table 1, no significant change was observed for the parameters, Dd, Ds, IVS, PW, FS, and EF. The results indicated that the contractility of LV was not affected, even though its apex was punc-

Table 1
Echocardiographic analyses at pre- and post-sonoporation

	Pre-transfection ($n = 5$)	Post-transfection ($n = 5$)	P
BW (g)	22.8 ± 0.37	22.8 ± 0.20	ns
IVSTd (mm)	0.54 ± 0.02	0.60 ± 0.03	ns
PWTd (mm)	0.62 ± 0.02	0.58 ± 0.02	ns
LVIDd (mm)	3.24 ± 0.02	3.28 ± 0.05	ns
LVIDs (mm)	2.34 ± 0.04	2.40 ± 0.06	ns
EF (%)	60.8 ± 2.15	61.0 ± 1.90	ns
FS (%)	26.8 ± 1.39	27.0 ± 1.27	ns

Cardiac function was not significantly affected by sonoporation-mediated transfection of pDNA/BR14. M-mode echocardiographic analysis was performed on mice before and 4 days after sonoporation at 2.0 W/50% PDR. BW, body weight; IVSTd, interventricular septum thickness; PWTd, LV posterior wall thickness; LVIDd, LV internal dimensions at end diastole; LVIDs, LV internal dimensions at end systole; EF, ejection fraction; FS, fractional shortening. Data are expressed as means ± SE.

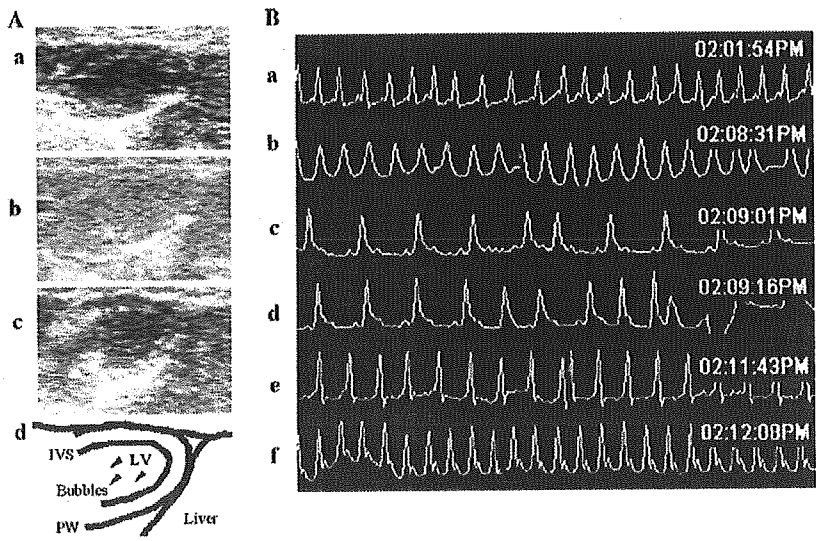

Fig. 1. (A) BR14 microbubbles were mostly disrupted by sonoporation, while some remained intact. C57BL/6 mice were injected with pGEG.GL3/BR14 into the LV. Shown are representative echocardiographic images before (a), immediately after (b), and 60 s after (c) the sonication at 2.0 W/50% PDR, while an echocardiographic image of (c) is illustrated schematically in (d). IVS, interventricular septum; PW, posterior wall. Arrowheads, intact microbubbles. (B) The transient arrhythmia caused by sonoporation. Mice received LV injection with pGEG.GL3/BR14, and sonoporation at 2.0 W/50% PDR was performed. Shown are representative ECG records before (a), and 0 s (b), 30 s (c), 45 s (d), 3 min (e), and 3.5 min (f) after the initiation of sonoporation.

tured on injection. The body weight of the mice did not significantly change following the sonoporation-mediated transfection.

Sonoporation remarkably facilitated cardiac gene transfer in mice

A mixture of pGEG.GL3 and BR14 was injected into the mice via their TV or LV. Ultrasound was directed at the chest at various output intensities and PDRs, and 2–7 days later Luc activity in the heart was measured. Representative data are shown in Fig. 2. When the mixture was injected into the LV, sonication at 2.0 W/50% PDR induced a significantly higher Luc activity on day 4 compared with that at 1.0 W/20% PDR (approximately 46-fold) or 1.0 W/50% PDR (approximately 13-fold). Transfection into the heart was more efficient when the mixture was injected into the LV than when it was injected into the TV. For example, compared with injection into the TV, expression was 67-fold higher 4 days following injection into the LV with sonoporation at 2.0 W/50% PDR. Optimal transfection was achieved by intra-LV injection and ultrasonication at 2.0 W/50% PDR, which resulted in Luc activity as high as approximately 6.0×10^4 RLU/mg protein/10 s on day 4, although the transgene activity was significantly decreased by day 7.

Transgene product was predominantly detected at subendocardial layer of the myocardium and anterior-septal wall of LV

To identify the localization of expression of the transferred gene, the heart was transfected with pGEG.β or pGEG.EGFP under the optimal conditions determined as described above. X-gal staining of the pGEG.β-transfected heart demonstrated that the β-gal was significantly expressed in the subendocardial layer of the LV and a part of the right ventricle. The strongest expression was detected at the anterior-septal wall of the LV that had faced the ultrasound probe (Fig. 3B). The pGEG.EGFP-transfected heart was examined histologically by fluorescence microscopy. The green fluorescence was observed in cardiomyocytes in the subendocardial layer (Figs. 3D and F). Consistent results were obtained by immunohistochemical staining of the pGEG.EGFP-transfected heart (data not shown). These findings indicated that transgene product was expressed in the subendocardial layer as well as in the anterior-septal wall of the LV.

Heart-specific transfection was achieved by sonoporation-based gene delivery

To investigate whether the present protocol allowed gene transfection in organs other than the heart, pGEG.GL3 was transfected as described above and the levels of Luc activity were determined quantitatively in lung, liver, kidney, spleen, intestine, ovary, and brain. Luc activity was not significantly increased in any of the organs tested (Fig. 4), indicating that the transfection procedure could deliver genes only to the heart.

Sonotransduction of siRNA induced specific gene silencing in coronary artery

We investigated whether the sonoporation-assisted DNA delivery procedure is also applicable to delivering siRNA into the heart. siRNA duplex specific for EGFP is capable of silencing the fluorescent protein in vivo, as demonstrated by preliminary experiments in which the siRNA was injected intravenously into EGFP TGM

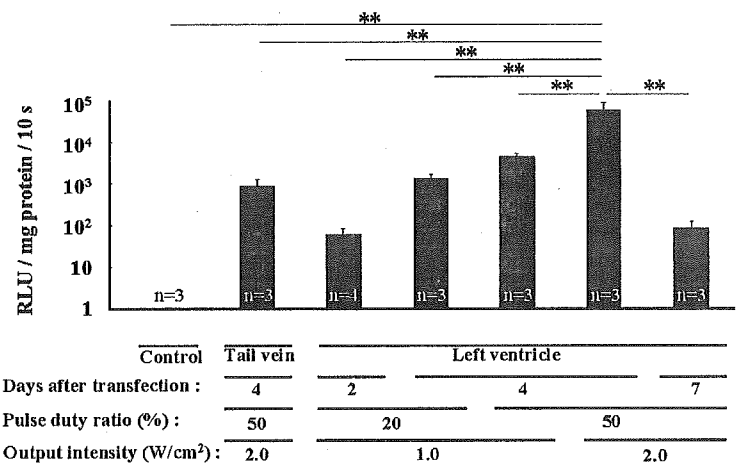

Fig. 2. Ultrasound-mediated transfection of pDNA under various conditions. pGEG.GL3/BR14 solution was injected into mice via the LV or TV route, and the heart was sonicated under the indicated conditions. Two, four, or seven days later, mice were sacrificed and Luc activities in the heart extracts were measured. Bars, SE. $^{**}P < 0.01$.

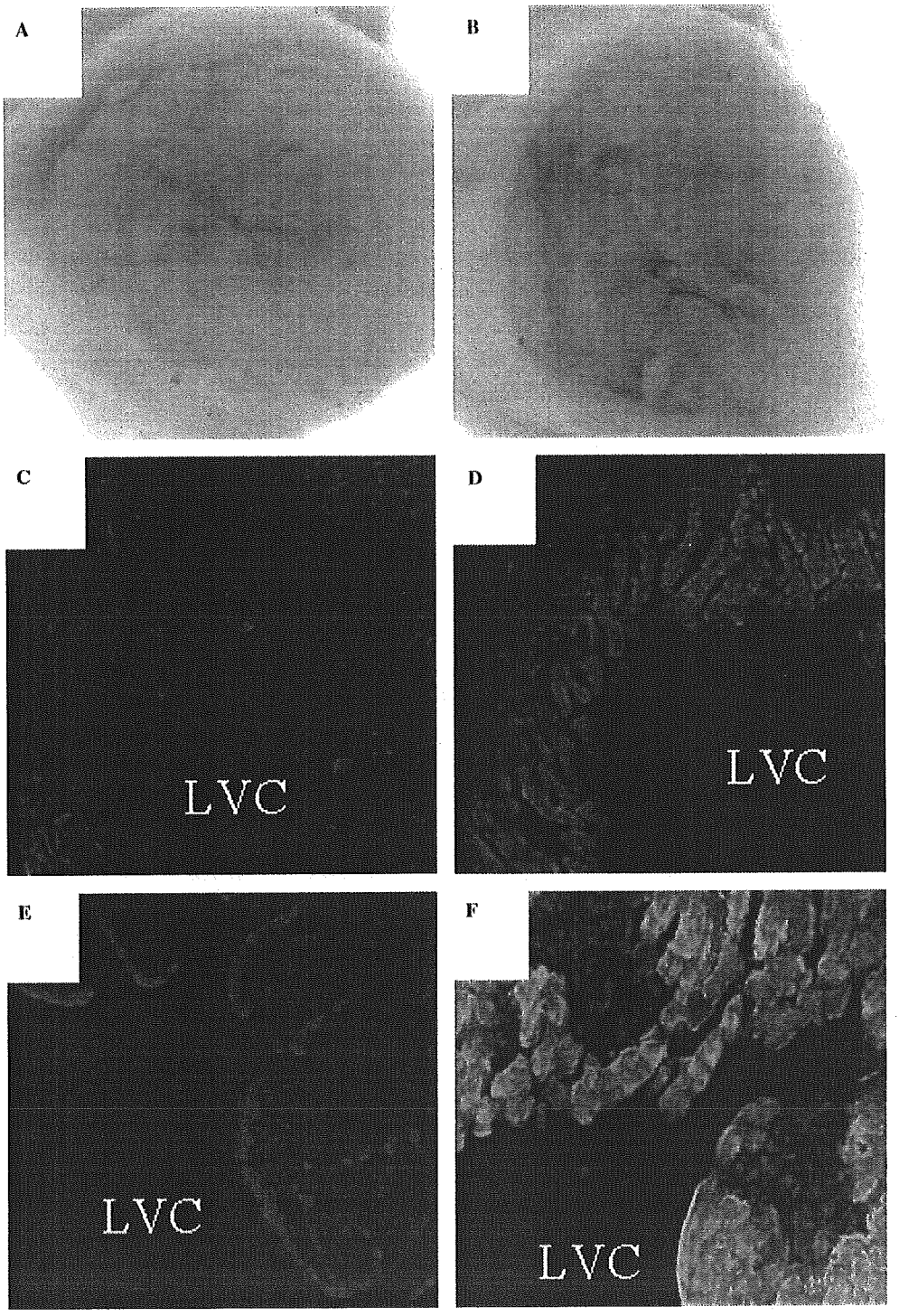

Fig. 3. Expression of transgene product in cardiomyocytes at the subendocardial layer and anterior-septal wall. Mice were given an intra-LV injection with pGEG.β/BR14, and sonication was performed at 2.0 W/50% PDR (B, D, and F). Control mice were left untreated (A, C, and E). Four days after the transfection, the hearts were excised. Shown are stereomicroscopic images of X-gal-stained cross-sections (A,B) and fluorescence microscopic images of cryosections (C–F). LVC, left ventricular cavity. Original magnifications were 4× (A,B), 40× (C,D), and 100× (E,F).

and expression of the transgene product was substantially suppressed in the hepatic parenchymal cells (Fig. 5B). siRNA was transfected into EGFP TGM, and the heart sections were observed by a fluorescence microscope. Representative findings are shown in Figs. 5C–F. In the control mice that received an injection of BR14 but not siRNA, the sonoporation procedure failed to affect EGFP expression in cardiomyocytes or coronary

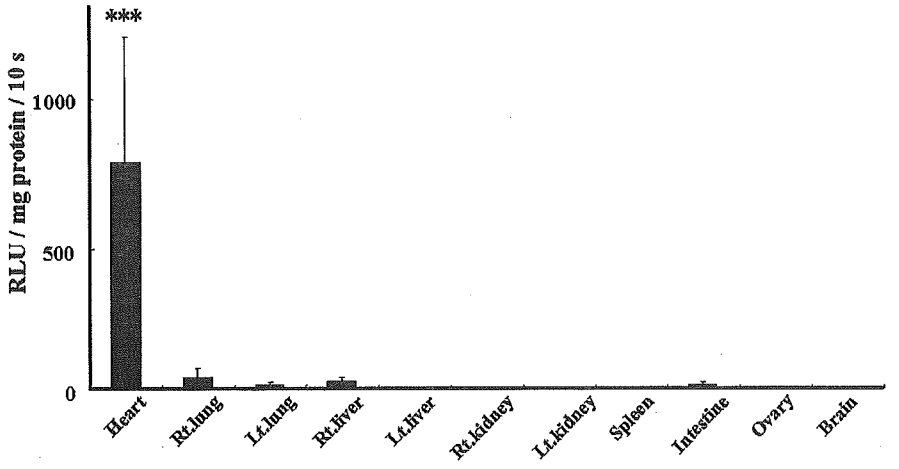

Fig. 4. Heart-specific pDNA transfer obtained by sonoporation-mediated transfection. Mice received an injection of pGEG.GL3/BR14 into the LV, and sonication was performed at 1.0 W/20% PDR. Four days later, the indicated organs were excised and Luc activity in each tissue extract was measured. Bars, SE. $***P < 0.001$ vs other organs ($n = 3$).

vessels (Figs. 5C and E). Intra-LV co-injection of siRNA-GFP and BR14 in combination with sonication at 1.0 W/10% PDR resulted in a substantial reduction of EGFP expression in the coronary artery wall 48 h after transduction, while cardiomyocytes were not influenced in terms of the intensity of the green fluorescence (Figs. 5D and F). The silencing of EGFP expression was detected not only at the main trunk of the left and right coronary arteries, but also at peripheral branches of the coronary arterial wall that could be identified by the structure of their vascular lumen. Similar results were also obtained by sonoporation performed under two other conditions, i.e., 1.0 W/10% PDR and 2.0 W/50% PDR (data not shown).

Discussion

Intra-LV injection of a mixture of an expression vector and the micobubble agent BR14 and concomitant ultrasonication resulted in significant expression of the marker gene in cardiomyocytes in the subendocardial layer and the antero-septal wall of the murine heart. BR14 also facilitated sonoporation-mediated transfer of siRNA duplex into the coronary artery, resulting in substantial gene silencing in vivo. Our study suggests an improved methodology for achieving safe and efficient genetic modification in the heart, in both gain-of-function and loss-of-function manners.

The present study also indicates that sonoporation-mediated pDNA transfer is strongly enhanced by the third-generation microbubble, BR14. BR14 is a negatively charged ultrasound contrast agent consisting of perfluorobutane-containing microbubbles stabilized by a phospholipid monolayer [20,34,35]. We also compared BR14 with Optison in sonoporation-mediated transfection into murine heart. An intra-TV injection of 500 μg pGEG.GL3/Optison and sonoporation at 2.0 W/50% PDR resulted in Luc expression in the cardiac muscle at a level similar to that when BR14 was used (1330 ± 310 RLU/mg protein/10 s on day 4 ($n = 9$)). However, some mice died immediately after receiving an intra-TV injection of Optison even without the sonoporation. Although Optison has been shown to be a useful agent for ultrasound-based transfection in rats and larger animals [9,12–14,17,18], BR14 may be more suitable in mice because a TV injection of BR14 did not kill any mice in the present study. The difference in results may be due to difference in the size of the agents: the mean diameter of BR14 is 2.5–3.0 μm, which is small compared with its predecessors [17,35,36]. The diameter of erythrocytes in C57BL/6 mice is about a half of that in humans (MCV 44.8 ± 0.26 fl, MCH 15.6 ± 0.49 pg, MCHC 34.7 ± 1.12 g/dl). Fisher et al. [36] examined the distribution of microbubbles intravenously administered into C57BL-6 mice. Intravital microscopic analyses demonstrated that neutral microbubbles larger than 4 μm in diameter persisted in capillaries in a size-dependent manner. Although the mean diameter of Optison is 2.0–4.5 μm, it contains bubbles up to 32 μm in diameter. These large bubbles may cause lethal embolisms in some vital organs in mice.

With regard to the routes of injection of pDNA/BR14, a higher rate of pDNA transfection was obtained by injection into the LV than by injection into the TV. These results suggest that high concentrations of pDNA and microbubble in coronary circulation are required at the time of sonication to achieve efficient sonoporation-based transfection.

In our study, pDNA could have reached the myocardium via 2 routes, i.e., directly from the LV cavity or through the coronary capillaries. This may explain why pDNA was predominantly delivered into the myocardium in the subendocardial layer and the anterior-septal

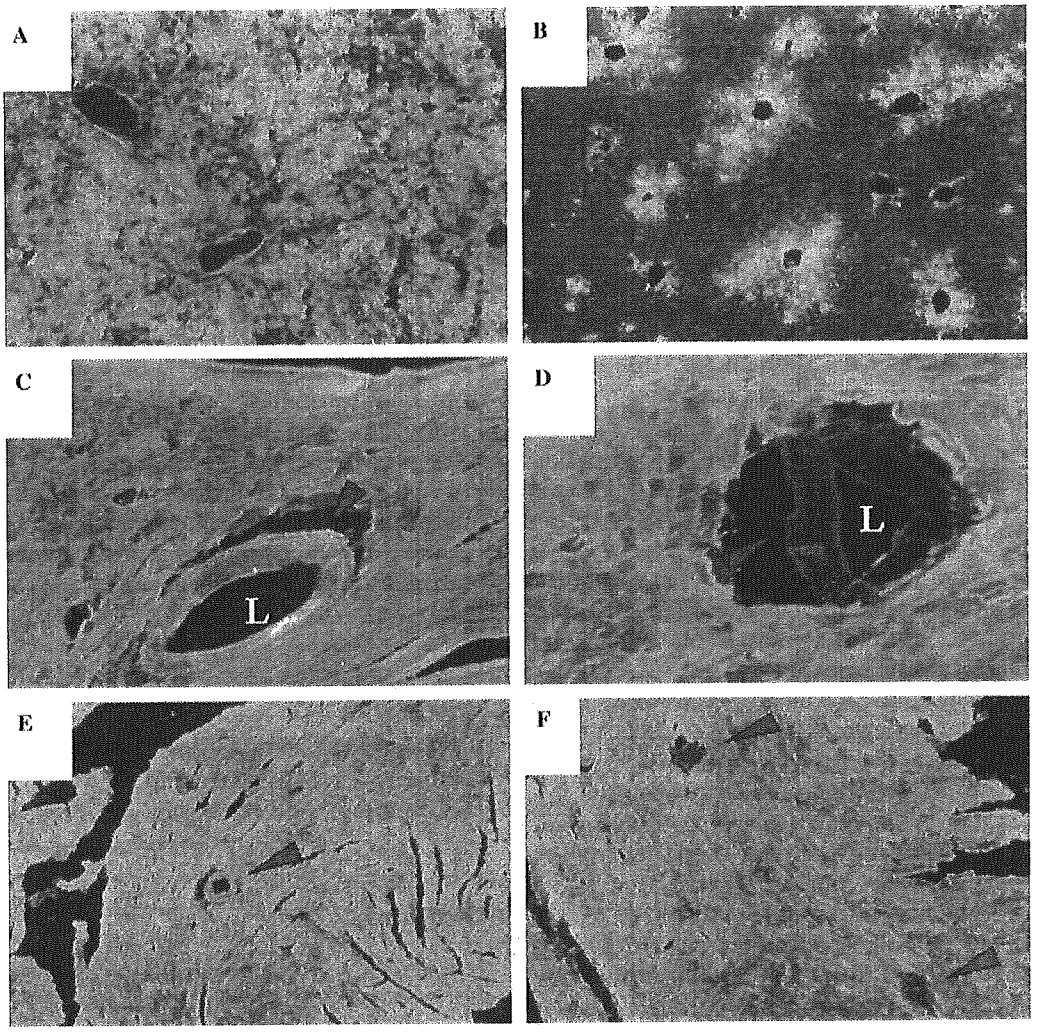

Fig. 5. Sonoporation-based transduction of siRNA silenced EGFP expression in the coronary arterial wall. (A) Fluorescence microscopic image of a liver section of EGFP-TGM. (B) EGFP-TGM were given a rapid tail vein injection with siRNA-GFP. Two days later, cryosections of the liver were observed under fluorescence microscope. (C–F) EGFP-TGM received an intra-LV injection of BR14 (C,E) or siRNA-GFP/BR14 (D,F), and sonication was performed at 1.0 W/10% PDR. Two days later, cryosections of the heart were observed under fluorescence microscope. Arrowheads in (C,D) indicate the left coronary artery, while those in (E,F) indicate the septal branches. L, lumen of arteries. Original magnifications were 100× (A,B), 200× (C,D), and 40× (E,F).

wall. Chen et al. [16] showed that the rate of pDNA transfection was significantly diminished by destroying microbubbles in the LV cavity before their entrance into the coronary microcirculation. So, presumably, the quantity of the pDNA transported via the coronary capillaries was greater than that delivered directly through the LV.

The present results showed that cardiomyocytes in the anterior-septal wall expressed the transgene more strongly than those in the inferior-posterior wall. The ultrasound beam is probably attenuated during passage through the cardiac muscle layers, so that the transfection efficiency may be inversely proportional to the distance from the probe. These results are consistent with the report by Chen et al. [16], who demonstrated that gene expression in the anterior wall was 2- to 2.5-fold greater than that in the posterior wall in rat heart transfected with pDNA by their sonoporation-mediated transduction protocols.

In the present study, maximum expression of transgene was obtained 4 days after transfection. This is consistent with a previous study in which expression levels peaked on day 4 following sonoporation-mediated transfer of pDNA and Optison into rat hearts [15].

In some previous studies, ultrasound-mediated destruction of Optison and other microbubbles induced rupture of microvessels at the sonicated site of the target organs [37,38]. In our experiments, a careful microscopic study did not demonstrate the RBC extravasation into the myocardium (data not shown). This is consistent

with echocardiographic examinations which demonstrated that cardiac contractility was not significantly affected after sonoporation (Table 1).

Some previous studies indicated that RNAi was induced in vitro into rat cardiomyocytes [39] as well as in human coronary vascular smooth muscle cells [40] in culture. We also demonstrated successful sequence-specific knockdown of endogenous gene expression in vivo in the coronary artery of adult mice using siRNA. RNAi may offer novel strategies for therapeutic molecular targeting, enabling artificial regulation of proteins that are responsible for the pathogenesis and/or progression of coronary diseases. For example, specific silencing of NF-κB or platelet-derived growth factor (PDGF) A-chain may suppress neointimal formation in coronary vasculature, which may have prophylactic implications for restenosis after coronary intervention as well as for the progression of atherosclerosis. These concepts are supported by previous studies in which balloon-injured artery models of animals were treated with decoy oligonucleotide that suppresses NF-κB activity [41] or a PDGF-targeting ribozyme [42].

It is noteworthy that pDNA was transfected effectively into cardiomyocytes, while the siRNA was transduced into coronary vascular wall. Although the precise mechanisms underlying these phenomena remain unclear, we propose the following explanation. Ultrasound-mediated cavitation may damage endothelial cells in both arteries and capillaries. Due to its small size, siRNA may easily diffuse from the bloodstream into tissue via endothelium when passing through the coronary arteries and arterioles, resulting in efficient transduction into arterial/arteriolar walls including the smooth muscle cells. Because pDNA permeates endothelium more slowly, transduction occurs less readily during its passage through arterioles. Instead, the pDNA is transduced predominantly at the capillary bed where cavitation from transient microbubbles is more intense. As a result, pDNA may be transfected into cardiomyocytes residing immediately beyond the extremely thin capillary wall.

To obtain further higher transduction efficacy, the following may be employed in combination with the sonoporatoin. Administration with the vascular endothelial growth factor (VEGF) may facilitate transfer of genetic materials through the endothelium, due to an increase in permeability of the endothelial cell membrane [43]. ECG-triggered sonication may also be effective because ultrasound-based cavitation can be generated precisely at the diastolic phase, when the coronary blood flow is higher than in the systolic phase. Use of RNase inhibitor [25] may prevent degradation of siRNA.

Kunichika et al. [20] showed that BR14 highlights ischemic risk areas in myocardium as a hyperenhanced "hot spot" when myocardial contrast echocardiography is performed following coronary reperfusion. Therefore, sonoporation using BR14 may enable targeted gene delivery to ischemic cardiomyocytes in patients with myocardial infarction, specifically delivering therapeutic nucleic acids into damaged cells.

Finally, it should be emphasized that the present procedure enables gene transfer and knockdown in the murine heart, although previous studies have documented ultrasound-assisted transfection into the hearts of larger animals, including rats [10,16] and dogs [11]. The mouse is a useful animal for post-genomic experimental cardiology. Particularly, a variety of transgenic and gene out mice have been established, providing extremely useful tools to elucidate the molecular mechanisms of cardiovascular disorders. The present method may be applied to these genetically engineered mice, providing a suitable technology to promote functional genomic analyses, as well as to examine candidate molecules for therapeutic molecular targeting for cardiovascular diseases.

Acknowledgment

This work was supported by a Grant-in-Aid for scientific research from the Japanese Ministry of Education, Culture, Sports, Science and Technology.

References

[1] M. Iwatate, Y. Gu, T. Dieterle, Y. Iwanaga, K.L. Peterson, M. Hoshijima, K.R. Chien, J. Ross, In vivo high-efficiency transcoronary gene delivery and Cre-LoxP gene switching in the adult mouse heart, Gene Ther. 10 (2003) 1814–1820.

[2] H.C. Champion, D. Georgakopoulos, S. Haldar, L. Wang, Y. Wang, D.A. Kass, Robust adenoviral and adeno-associated viral gene transfer to the in vivo murine heart: application to study of phospholamban physiology, Circulation 108 (2003) 2790–2797.

[3] K. Li, R.E. Welikson, K.L. Vikstrom, L.A. Leinwand, Direct gene transfer into the mouse heart, J. Mol. Cell. Cardiol. 29 (1997) 1499–1504.

[4] H. Lin, M.S. Parmacek, G. Morle, S. Bolling, J.M. Leiden, Expression of recombinant genes in myocardium in vivo after direct injection of DNA, Circulation 82 (1990) 2217–2221.

[5] R.N. Kitsis, P.M. Buttrick, E.M. McNally, M.L. Kaplan, L.A. Leinwand, Hormonal modulation of a gene injected into rat heart in vivo, Proc. Natl. Acad. Sci. USA 88 (1991) 4138–4142.

[6] K. Tomiyasu, Y. Oda, M. Nomura, E. Satoh, S. Fushiki, J. Imanishi, M. Kondo, O. Mazda, Direct intra-cardiomuscular transfer of beta2-adrenergic receptor gene augments cardiac output in cardiomyopathic hamsters, Gene Ther. 7 (2000) 2087–2093.

[7] K. Ogawa, K. Tachibana, T. Uchida, T. Tai, N. Yamashita, N. Tsujita, R. Miyauchi, High-resolution scanning electron microscopic evaluation of cell-membrane porosity by ultrasound, Med. Electron Microsc. 34 (2001) 249–253.

[8] D.L. Miller, S.V. Pislaru, J.E. Greenleaf, Sonoporation: mechanical DNA delivery by ultrasonic cavitation, Somat. Cell Mol. Genet. 27 (2002) 115–134.

[9] T. Li, K. Tachibana, M. Kuroki, M. Kuroki, Gene transfer with echo-enhanced contrast agents: comparison between Albunex, Optison, and Levovist in mice-initial results, Radiology 229 (2003) 423–428.
[10] R.V. Shohet, S. Chen, Y.T. Zhou, Z. Wang, R.S. Meidell, R.H. Unger, P.A. Grayburn, Echocardiographic destruction of albumin microbubbles directs gene delivery to the myocardium, Circulation 101 (2000) 2554–2556.
[11] M. Vannan, T. McCreery, P. Li, Z. Han, E. Unger, B. Kuersten, E. Nabel, S. Rajagopalan, Ultrasound-mediated transfection of canine myocardium by intravenous administration of cationic microbubble-linked plasmid DNA, J. Am. Soc. Echocardiogr. 15 (2002) 214–218.
[12] M. Blomley, Which US microbubble contrast agent is best for gene therapy? Radiology 229 (2003) 297–298.
[13] S. Miura, K. Tachibana, T. Okamoto, K. Saku, In vitro transfer of antisense oligodeoxynucleotides into coronary endothelial cells by ultrasound, Biochem. Biophys. Res. Commun. 298 (2002) 587–590.
[14] Y. Taniyama, K. Tachibana, K. Hiraoka, T. Namba, K. Yamasaki, N. Hashiya, M. Aoki, T. Ogihara, K. Yasufumi, R. Morishita, Local delivery of plasmid DNA into rat carotid artery using ultrasound, Circulation 105 (2002) 1233–1239.
[15] R. Bekeredjian, S. Chen, P.A. Frenkel, P.A. Grayburn, R.V. Shohet, Ultrasound-targeted microbubble destruction can repeatedly direct highly specific plasmid expression to the heart, Circulation 108 (2003) 1022–1026.
[16] S. Chen, R.V. Shohet, R. Bekeredjian, P. Frenkel, P.A. Grayburn, Optimization of ultrasound parameters for cardiac gene delivery of adenoviral or plasmid deoxyribonucleic acid by ultrasound-targeted microbubble destruction, J. Am. Coll. Cardiol. 42 (2003) 301–308.
[17] S. Mayer, P.A. Grayburn, Myocardial contrast agents: recent advances and future directions, Prog. Cardiovasc. Dis. 44 (2001) 33–44.
[18] R. Bekeredjian, P.A. Grayburn, R.V. Shohet, Use of ultrasound contrast agents for gene or drug delivery in cardiovascular medicine, J. Am. Coll. Cardiol. 45 (2005) 329–335.
[19] N.G. Fisher, H. Leong-Poi, T. Sakuma, S.J. Rim, J.P. Bin, S. Kaul, Detection of coronary stenosis and myocardial viability using a single intravenous bolus injection of BR14, J. Am. Coll. Cardiol. 39 (2002) 523–529.
[20] H. Kunichika, B. Peters, B. Cotter, H. Masugata, N. Kunichika, P.L. Wolf, A.N. DeMaria, Visualization of risk-area myocardium as a high-intensity, hyperenhanced "hot spot" by myocardial contrast echocardiography following coronary reperfusion: quantitative analysis, J. Am. Coll. Cardiol. 42 (2003) 552–557.
[21] Y. Sakakima, S. Hayashi, Y. Yagi, A. Hayakawa, K. Tachibana, A. Nakao, Gene therapy for hepatocellular carcinoma using sonoporation enhanced by contrast agents, Cancer Gene Ther. (in press).
[22] E.F. Akowuah, C. Gray, A. Lawrie, P.J. Sheridan, C.H. Su, T. Bettinger, A.F. Brisken, J. Gunn, D.C. Crossman, S.E. Francis, A.H. Baker, C.M. Newman, Ultrasound-mediated delivery of TIMP-3 plasmid DNA into saphenous vein leads to increased lumen size in a porcine interposition graft model, Gene Ther. 12 (2005) 1154–1157.
[23] G.J. Hannon, RNA interference, Nature 418 (2002) 244–251.
[24] J. Downward, RNA interference, Br. Med. J. 328 (2004) 1245–1248.
[25] A.P. McCaffrey, L. Meuse, T.T. Pham, D.S. Conklin, G.J. Hannon, M.A. Kay, RNA interference in adult mice, Nature 418 (2002) 38–39.
[26] D.L. Lewis, J.E. Hagstrom, A.G. Loomis, J.A. Wolff, H. Herweijer, Efficient delivery of siRNA for inhibition of gene expression in postnatal mice, Nat. Genet. 32 (2002) 107–108.
[27] T. Kishida, H. Asada, S. Gojo, S. Ohashi, M. Shin-Ya, K. Yasutomi, R. Terauchi, K.A. Takahashi, T. Kubo, J. Imanishi, O. Mazda, Sequence-specific gene silencing in murine muscle induced by electroporation-mediated transfer of short interfering RNA, J. Gene. Med. 6 (2004) 105–110.
[28] F.D. Cui, T. Kishida, S. Ohashi, H. Asada, K. Yasutomi, E. Satoh, T. Kubo, S. Fushiki, J. Imanishi, O. Mazda, Highly efficient gene transfer into murine liver achieved by intravenous administration of naked Epstein–Barr virus (EBV)-based plasmid vectors, Gene Ther. 8 (2001) 1508–1513.
[29] T. Kishida, H. Asada, Y. Itokawa, F.D. Cui, M. Shin-Ya, S. Gojo, K. Yasutomi, Y. Ueda, H. Yamagishi, J. Imanishi, O. Mazda, Interleukin (IL)-21 and IL-15 genetic transfer synergistically augments therapeutic antitumor immunity and promotes regression of metastatic lymphoma, Mol. Ther. 8 (2003) 552–558.
[30] H. Nakanishi, O. Mazda, E. Satoh, H. Asada, H. Morioka, T. Kishida, M. Nakao, Y. Mizutani, A. Kawauchi, M. Kita, J. Imanishi, T. Miki, Nonviral genetic transfer of Fas ligand induced significant growth suppression and apoptotic tumor cell death in prostate cancer in vivo, Gene Ther. 10 (2003) 434–442.
[31] O. Mazda, Improvement of nonviral gene therapy by Epstein–Barr virus (EBV)-based plasmid vectors, Curr. Gene. Ther. 2 (2002) 379–392.
[32] S. Ohashi, T. Kubo, T. Kishida, T. Ikeda, K. Takahashi, Y. Arai, R. Terauchi, H. Asada, J. Imanishi, O. Mazda, Successful genetic transduction in vivo into synovium by means of electroporation, Biochem. Biophys. Res. Commun. 293 (2002) 1530–1535.
[33] K. Tomiyasu, E. Satoh, Y. Oda, K. Nishizaki, M. Kondo, J. Imanishi, O. Mazda, Gene transfer in vitro and in vivo with Epstein–Barr virus-based episomal vector results in markedly high transient expression in rodent cells, Biochem. Biophys. Res. Commun. 253 (1998) 733–738.
[34] H. Takeuchi, K. Ohmori, I. Kondo, K. Shinomiya, A. Oshita, Y. Takagi, J. Yoshida, K. Mizushige, M. Kohno, Interaction with leukocytes: phospholipid-stabilized versus albumin-shell microbubbles, Radiology 230 (2004) 735–742.
[35] N.G. Fisher, J.P. Christiansen, H. Leong-Poi, A.R. Jayaweera, J.R. Lindner, S. Kaul, Myocardial and microcirculatory kinetics of BR14, a novel third-generation intravenous ultrasound contrast agent, J. Am. Coll. Cardiol. 39 (2002) 530–537.
[36] N.G. Fisher, J.P. Christiansen, A. Klibanov, R.P. Taylor, S. Kaul, J.R. Lindner, Influence of microbubble surface charge on capillary transit and myocardial contrast enhancement, J. Am. Coll. Cardiol. 40 (2002) 811–819.
[37] D.L. Miller, J. Quddus, Diagnostic ultrasound activation of contrast agent gas bodies induces capillary rupture in mice, Proc. Natl. Acad. Sci. USA 97 (2000) 10179–10184.
[38] R.J. Price, D.M. Skyba, S. Kaul, T.C. Skalak, Delivery of colloidal particles and red blood cells to tissue through microvessel ruptures created by targeted microbubble destruction with ultrasound, Circulation 98 (1998) 1264–1267.
[39] A. Watanabe, M. Arai, M. Yamazaki, N. Koitabashi, F. Wuytack, M. Kurabayashi, Phospholamban ablation by RNA interference increases Ca^{2+} uptake into rat cardiac myocyte sarcoplasmic reticulum, J. Mol. Cell. Cardiol. 37 (2004) 691–698.
[40] F. Blaschke, D. Bruemmer, F. Yin, Y. Takata, W. Wang, M.C. Fishbein, T. Okura, J. Higaki, K. Graf, E. Fleck, W.A. Hsueh, R.E. Law, C-reactive protein induces apoptosis in human coronary vascular smooth muscle cells, Circulation 110 (2004) 579–587.
[41] K. Yamasaki, T. Asai, M. Shimizu, M. Aoki, N. Hashiya, H. Sakonjo, H. Makino, Y. Kaneda, T. Ogihara, R. Morishita, Inhibition of NFkappaB activation using cis-element 'decoy' of NFkappaB binding site reduces neointimal formation in porcine balloon-injured coronary artery model, Gene Ther. 10 (2003) 356–364.